Ultrahigh-potent and broadly neutralizing anti-CD4 trimeric nanobodies inhibit HIV-1 infection by inducing CD4 conformational alteration

Xilin Wu (xilinwu@nju.edu.cn)
Nanjing Uiniversity https://orcid.org/0000-0002-2829-6654

Linjing Zhu
Center for Public Health Research, Medical School, Nanjing University, Nanjing

Xiangyao Wang
Tianjin Key Laboratory of Function and Application of Biological Macromolecular Structures, School of Life sciences, Tianjin University,

Fengfeng Ni
State Key Laboratory of Virology, Wuhan Institute of Virology, Center for Biosafety Mega-Science, Chinese Academy of Sciences

Mingjun Ao
State Key Laboratory of Coordination Chemistry, Nanjing University https://orcid.org/0009-0007-4831-7532

Ruoke Wang
Comprehensive AIDS Research Center, Center for Global Health and Infectious Diseases Research, NexVac Research Center, Center for Infectious Diseases Research, Department of Basic Medical Sciences,

Bin Zheng
State Key Laboratory of Coordination Chemistry, Nanjing University

Chen Chen
Department of Infection, Nanjing Hospital Affiliated to Nanjing university of Chinese Medicine

Linen Shi
Center for Public Health Research, Medical School, Nanjing University

Shengya Geng
Center for Public Health Research, Medical School, Nanjing University

Jiaqian Hu
Center for Public Health Research, Medical School, Nanjing University

Mengshi Yang
State Key Laboratory of Virology, Wuhan Institute of Virology, Center for Biosafety Mega-Science, Chinese Academy of Sciences

Doudou Zhang
Center for Public Health Research, Medical School, Nanjing University

Ping Yang
State Key Laboratory of Virology, Wuhan Institute of Virology, Center for Biosafety Mega-Science, Chinese Academy of Sciences
Miaomiao Li
State Key Laboratory of Virology, Wuhan Institute of Virology, Center for Biosafety Mega-Science, Chinese Academy of Sciences
Yuncheng Li
State Key Laboratory of Virology, Wuhan Institute of Virology, Center for Biosafety Mega-Science, Chinese Academy of Sciences
Qinxue Hu
Wuhan Institute of Virology, Chinese Academy of Sciences
Sheng Ye
Tianjin University https://orcid.org/0000-0001-9300-6257
Peng Zheng
State Key Laboratory of Coordination Chemistry, Nanjing University
Hongxia Wei
Department of Infection, Nanjing Hospital Affiliated to Nanjing university of Chinese Medicine
Linqi Zhang
Tsinghua University https://orcid.org/0000-0003-4931-509X
Yalan Liu
Wuhan Institute of Virology
Zhiwei Wu
Nanjing University https://orcid.org/0000-0002-0672-948X

Article

Keywords:

Posted Date: November 7th, 2023

DOI: https://doi.org/10.21203/rs.3.rs-3443144/v1

Additional Declarations: There is **NO** Competing Interest.

Abstract

Despite substantial progress in antiretroviral therapy (ART) effectively suppressing HIV-1 replication in the bloodstream, a cure for HIV remains elusive. Existing antiviral drugs pose limitations, including lifelong medication, frequent administration, side effects, and viral resistance, necessitating novel HIV-1 treatment approaches. CD4, the primary receptor for HIV-1 entry into host cells, was once a prime target for drug or vaccine development. However, challenges, such as the potency and breadth of neutralization and cytotoxicity associated with anti-CD4 antibodies, hindered progress. Nevertheless, Ibalizumab, the sole approved CD4-specific antibody for HIV-1 treatment, reignited interest in exploring alternative anti-HIV targets, emphasizing CD4's potential value for effective drug development. Here, we investigated anti-CD4 nanobodies, with a focus on Nb457 isolated from a human CD4-immunized alpaca. Nb457 displayed remarkable ultra-high potency and broad-spectrum activity against HIV-1, surpassing Ibalizumab's efficacy. Importantly, Nb457 showed no impact on $CD4^+$ T cell function, akin to Ibalizumab. Strikingly, engineered trimeric Nb457 nanobodies, Nb_{457}-Nb_{HSA}-Nb_{457}, achieved 100% inhibition against live HIV-1, outperforming Ibalizumab and parental Nb457. Structural analysis revealed that Nb457 binding induced a CD4 conformational change, impeding viral entry. Molecular Dynamics simulations elucidated the structural basis for the complete inhibition of HIV-1 by Nb_{457}-Nb_{HSA}-Nb_{457}. Furthermore, Nb457 exhibited significant therapeutic efficacy against HIV-1 infection in humanized mouse models. In conclusion, our study highlights ultra-potent anti-CD4 nanobodies as a compelling source of new HIV-1 therapeutics. The development of Nb457-based drugs holds the potential to revolutionize clinical HIV-1 treatment, providing a powerful tool in the battle against this persistent global health challenge.

Highlights

1. Nb457, isolated from a human CD4-immunized alpaca, displayed remarkable ultra-high potency and broad-spectrum activity against HIV-1, surpassing Ibalizumab's efficacy.
2. Structural analysis revealed that Nb457 binding induced a CD4 conformational change, effectively impeding viral entry.
3. Nb457 trimeric nanobodies achieved 100% inhibition against live HIV-1 virus, outperforming Ibalizumab and parental Nb457.
4. Nb457 trimeric nanobodies demonstrated significant therapeutic efficacy against HIV-1 infection in humanized mouse models.

Introduction

Although antiretroviral therapy (ART) has been efficacious in controlling HIV-1 replication over extended periods, it is not a curative treatment and requires lifelong administration[1]. The emergence of HIV-1 drug resistance has become increasingly prevalent, with untreated patients experiencing an estimated 7–19% prevalence of resistance to non-nucleoside reverse transcriptase inhibitors (NNRTIs) (known as transmitted drug resistance) and a much higher prevalence of 50–80% for NNRTIs in patients who have

received ART[2,3]. Hence, potent broadly neutralizing antibodies (bNAbs) have emerged as a promising alternative or complementary approach for HIV-1 immunotherapy[4]. Nevertheless, bNAbs targeting the HIV-1 envelope spike may be susceptible to antibody resistance, potentially limiting their clinical efficacy[5]. In contrast, CD4, which serves as the primary host receptor for HIV-1 entry, represents a promising target for HIV-1 treatment. However, antibodies targeting CD4 with potent neutralization and low cytotoxicity are rare and thus only one such a drug is currently available in the market. Ibalizumab, a humanized IgG4 antibody targeting CD4, was approved as the pioneering antibody drug for the treatment of multidrug-resistant HIV-1 by the FDA in 2018[6,7]. Compared to traditional chemical drugs, Ibalizumab can be administered at long intervals, with a dosing frequency of once every 14 days[6,7]. In addition, we previously engineered a single-gene-encoded bispecific broadly neutralizing antibody, BiIA-SG, by combining two single-chain variable fragment (scFv) binding domains of Ibalizumab and a broadly neutralizing antibody, PGT-128, which targets HIV-1 gp120[8]. BiIA-SG demonstrated substantial improvements in breadth and potency, leading to functional cure in humanized mouse and macaque models, thereby highlighting the value of CD4 antibodies for the development of novel therapeutics against HIV-1 [8,9].

Although Ibalizumab holds promise as an HIV-1 treatment, its clinical efficacy is limited by its relatively limited breadth and potency, which may lead to the emergence of viral escape during treatment. Additionally, Ibalizumab is a humanized monoclonal antibody derived from mice, which may have a high degree of immunogenicity during long-term administration. In addition, the high production costs associated with Ibalizumab may present a substantial obstacle to its long-term clinical use, which could limit its broad adoption.

Nanobodies have garnered significant interest in the development of new drugs, given their advantages and potentials over traditional antibodies. Derived from the Camelidae family, nanobodies constitute the smallest naturally functional antibody fragment available to date [10–13], making it possible to create multi-targeted antibodies. Furthermore, nanobodies exhibit exceptional stability, even when administered subcutaneously. Our previous results indicated that nanobody remained 100% activity even after prolonged exposure to high temperatures, such as 70 ^{o}C for an hour, and room temperature for two months, or after five rounds of repeated freezing and thawing [14,15]. In addition, recent findings have demonstrated that nanobodies can be efficiently produced in yeast, reducing the production cost considerably[12]. Importantly, our data, as well as other reports, indicated that nanobodies offered a unique binding mode to target proteins when compared to traditional antibodies, leading to remarkably potent neutralization against viral infections[15–17]. Following the approval of Caplacizumab, the first camel-derived nanobody, for marketing in 2018[18], numerous nanobodies currently have been in clinical trials including ALX-0651 for tumors, ALX-0171 for RSV virus, and ALX for inflammation[12,13,19], underscoring the significant therapeutic potential of nanobodies. Thus far, anti-CD4 nanobodies have been developed and utilized for *in vivo* CD4 cell tracing[20], while no anti-CD4 nanobodies have yet been developed for the therapeutic purpose of neutralizing HIV-1 infection.

The present study reported the isolation of anti-CD4 nanobodies from an alpaca that had been immunized with human CD4 protein. Following the isolation, the nanobodies were characterized and evaluated for their ability to neutralize HIV-1 infection using a panel of 93 different viral strains. One broadly neutralizing nanobody, Nb457, was identified and subjected to structural analysis. The findings from the crystal structure analysis revealed that the binding of Nb457 induced the alteration of CD4's conformation, which impaired HIV-1 gp120 binding to CD4, thus preventing viral entry into host cells. Moreover, the anti-HIV activity of Nb457 or Nb457-based trimeric nanobodies was evaluated in a humanized mouse model. The results offered evidence that Nb457 exhibited exceptional potency against diverse HIV-1 genotypes without discernible cytotoxicity. The study calls for the development of Nb457-based nanobody drug for HIV-1 treatment.

Results

CD4-induced anti-sera potently inhibited HIV-1 pseudovirus.

The high-titer anti-sera obtained from the third and fourth immunizations, with titers of 3.6×10^5 and 1.1×10^6, respectively, indicated that CD4-rFc was capable of inducing a strong immune response in the alpaca after the fourth immunization (Fig. 1A-C). To assess the neutralizing activity of the anti-sera against HIV-1 infection, a panel of diverse HIV-1 pseudovirus strains representing different subtypes that were isolated from both chronic and acute stages of infection were selected for neutralization assay. Following the fourth immunization, the anti-sera (4th anti-sera) demonstrated remarkably potent neutralizing activity against all 13 representative HIV-1 pseudoviruses, with an average 50% inhibitory dilution (ID_{50}) value of 9165, and neutralized 12 out of 13 pseudoviruses, achieving an average 90% inhibitory dilution (ID_{90}) value of 931 (Fig. 1D and E). These results suggest that the CD4-induced anti-sera possess broad and potent neutralizing activities against HIV-1 infection, thus providing a foundation for the subsequent isolation of anti-CD4 neutralizing nanobodies.

The isolation and characterization of anti-CD4 nanobodies

To isolate anti-CD4 nanobodies, a phage library displaying nanobodies was constructed from peripheral blood mononuclear cells (PBMC) obtained from the final immunization. The phage library had a diversity and in-frame rate exceeding 90%, and a size of 1.6×10^9, indicating high-quality establishment (Supplementary Fig. 1A). The CD4-his protein was utilized to enrich the library for three rounds, and single phage clones were selected from the enriched library for phage ELISA testing (Supplementary Fig. 1B). Results indicated that 30 out of 40 and 41 out of 46 clones were positive binders in the second and third enriched libraries, respectively, validating the enrichment process (Supplementary Fig. 1C). Consequently, a bacterial library was constructed based on the enriched phage library to obtain secreted nanobodies for characterization. Among 1920 single clones picked, 429 were positive binders on ELISA (Fig. 2A). Notably, 47 of these binders displayed neutralization activity against HIV-1 infection (Fig. 2B). Sequence

alignment of the 429 positive binders and the 47 neutralizers revealed high diversity in the positive binders (Fig. 2C and Supplementary Fig. 1D).

To further characterize the anti-CD4 nanobodies, we expressed them in 293F cells in the VHH-fused human Fc4 format (Fig. 2D). Notably, 29 out of 47 cell supernatants were able to bind to CD4 and effectively neutralize over 50% of HIV-1 infection (Fig. 2E, Supplementary Fig. 2 and Supplementary Table 1). Furthermore, 31 of the nanobodies exhibited affinities in the nanomolar range when measured for their binding affinity to CD4 (Fig. 2F and Supplementary Table 1). Based on these results and sequence analysis, we purified five nanobodies with distinct sequences (Nb_{319}-Fc, Nb_{434}-Fc, Nb_{457}-Fc, Nb_{505}-Fc, and Nb_{606}-Fc) for further evaluation of their neutralizing activity against representative HIV-1 pseudoviruses. Of these, Nb_{434}-Fc and Nb_{457}-Fc were found to be the most effective based on their neutralizing curve (Fig. 2G). SDS-PAGE analysis showed that Nb_{434}-Fc and Nb_{457}-Fc were of high purity (Supplementary Fig. 3A), and they were observed to preferentially bind to native CD4 protein in non-reduced conditions, indicating their interaction with a conformational epitope (Supplementary Fig. 3B). The binding curves of Nb_{457}-Fc and the reference antibody Ibalizumab in the Fc4 format were similar, with EC_{50} values of ~ 0.5μg/ml, outperforming Nb_{434}-Fc with an EC_{50} value of 1.899 μg/ml (Supplementary Fig. 4).

Furthermore, these nanobodies were also found to recognize human CD4 cells, both on the spleen of humanized NDG-HuPBL mice, as observed through immunofluorescence staining (Supplementary Fig. 5), and in PBMC obtained from healthy donors, as assessed by flow cytometry (Supplementary Fig. 6). In order to elucidate the binding kinetics of these nanobodies with CD4, Bio-Layer Interferometry (BLI) was employed as the analytical method. The equilibrium dissociation constants (KD) for Nb_{434}-Fc, Nb_{457}-Fc, and Ibalizumab were 0.216 nM, 0.026 nM, and < 0.001 nM, respectively. Furthermore, the association constants (Ka) for Nb_{434}-Fc, Nb_{457}-Fc, and Ibalizumab were measured as 1.64 x 10^7 $M^{-1}s^{-1}$, 2.89 x 10^7 $M^{-1}s^{-1}$, and 1.2 x 10^6 $M^{-1}s^{-1}$, respectively (Supplementary Fig. 7A-D).

Nb_{434}-Fc and Nb_{457}-Fc broadly neutralized HIV-1 infection in vitro

To evaluate the neutralizing activity of the anti-CD4 nanobodies Nb_{434}-Fc and Nb_{457}-Fc, we conducted analysis using a panel of 35 HIV-1 pseudoviruses that included isolates from multiple clades, covering major global HIV-1 subtypes CRF01_AE, B, B', CRF07_BC, CRF08_BC, B'C, and C. This panel comprised 13 acute or transmitted/founder viruses and 22 viruses isolated from chronic infections (Supplementary Table 2). Since nanobodies have smaller molecular weights than regular antibodies like Ibalizumab, we compared the equimolar concentration (pM) of each and showed that both Nb_{434}-Fc (with median IC_{50} and IC_{90} values of 10.8 pM and 80.4 pM, respectively) and Nb_{457}-Fc (with median IC_{50} and IC_{90} values of 4.94 pM and 33.23 pM, respectively) were significantly more effective than Ibalizumab (with median IC_{50} and IC_{90} values of 14.99 pM and 2614.3 pM, respectively) (Fig. 3A and B).

Overall, all three antibodies demonstrated substantial inhibitory activity, attaining 50% neutralization in all tested pseudoviruses (Fig. 3A and Supplementary Table 2). Intriguingly, Nb434-Fc and Nb_{457}-Fc achieved 90% inhibition of infection in 100% and 91.4% of tested pseudoviruses, respectively, compared to Ibalizumab, which achieved 90% inhibition of infection in only 54.2% of tested pseudoviruses (Fig. 3B and Supplementary Table 2). Furthermore, we found that all 17 Ibalizumab-resistant pseudoviruses could be neutralized by Nb_{434}-Fc, and 14 out of 17 Ibalizumab-resistant pseudoviruses could be neutralized by Nb_{457}-Fc (Fig. 3C and Supplementary Table 2). Additionally, we observed that these three antibodies exhibited varied potency against different subtypes of HIV-1 pseudovirus (Fig. 3D-F and Supplementary Fig. 8A-C). For example, Ibalizumab failed to neutralize all the tested B'C viruses, while Nb_{434}-Fc and Nb_{457}-Fc neutralized 100% and 50% of them, respectively, with an IC_{90} value of < 100 pM (Fig. 3D-F). Furthermore, Ibalizumab neutralized only 50% of tested subtype AE viruses with an IC_{90} value of 1000 pM-10,000 pM, while Nb_{434}-Fc and Nb_{457}-Fc neutralized 100% and 75% of the tested subtype AE viruses with IC_{90} values of < 100 pM, respectively (Fig. 3D-F). Particularly striking was Nb457's exceptional potency across almost various subtypes, attaining IC_{90} values below 100 pM (Fig. 3E).

Our findings suggest that Nb_{434}-Fc and Nb_{457}-Fc exhibit more potent and broad neutralization than Ibalizumab. Furthermore, these two nanobodies and Ibalizumab were also tested independently in a collaborative laboratory at Tsinghua University against a panel of 58 HIV-1 pseudoviruses, with average IC_{90} values of 0.1030 μg/ml (0.1288 nM) and 0.1026 μg/ml (0.1283 nM), respectively, while Ibalizumab exhibited an average IC_{90} value of 2.4858 μg/ml (1.6572 nM) (Supplementary Table 3). In this experiment, Ibalizumab neutralized only 60.3% (25/58) of the pseudoviruses with IC_{90} values of less than 50 μg/ml (33.33 nM), while Nb_{434}-Fc and Nb_{457}-Fc neutralized 100% and 96% (56/58) of the tested viruses, respectively (Supplementary Table 3), in agreement with our lab's findings (Fig. 3 and Supplementary Table 2).

Collectively, our findings provide compelling evidence that both Nb_{434}-Fc and Nb_{457}-Fc exhibit superiority over Ibalizumab, showcasing significantly improved average IC_{90} values and broader neutralization breadth.

Structural analysis of Nb457 binding to CD4

Nb_{457}-Fc displays exceptional binding affinity and superior neutralizing potency compared to Nb_{434}-Fc (Fig. 3B and Supplementary Fig. 7A-B), making it the preferred candidate for subsequent in-depth characterization and evaluation. To elucidate the molecular mechanisms underlying the potent neutralization of HIV-1 by Nb457, we determined the crystal structure of the Nb457-D1D2 of CD4 complex at a resolution of 1.78 Å (PDB: 8W90, Supplementary Table 4). The buried surface area (BSA) was 700 $Å^2$ and a total of 18 residues of CDRs constituted the epitope (Fig. 4A-B). Additionally, we identified several other residues within the D1-D2 of CD4, including K1, N32, S79, E92 in the D1, and P122, G123, S125 and Q163 in the D2 of CD4, which were involved in the hydrophobic interactions on binding interface (Fig. 4C). Furthermore, our analysis revealed that the CDR2 and CDR3 domains of Nb457 were the main

contributors to the interaction with the D1 and D2 domains of CD4, with key hydrogen bonds including W53, Y57, N59, D62 in CDR2, and S104 and Y106 in CDR3 (Fig. 4D-E and Supplementary Fig. 9A). To further explore the mechanism by which Nb457 inhibits HIV-1 entry into CD4 cells, we aligned the CD4-Nb457 complex with the CD4-gp120 complex of HIV-1. Our results showed that the binding site of Nb457 was distal to that of gp120, Moreover, the interaction of Nb457 with CD4 induced a substantial conformational change of loops on D1 and the major hydrogen bond interactions were reduced from 14 to 6, thus directly impairs gp120's binding to CD4 (Fig. 4F-H, Supplementary Fig. 9A-C and Supplementary Fig. 10A). Notably, when we compared the structural complex of Nb457 with that of Ibalizumab, we observed partial overlap in the epitope (Supplementary Fig. 10B), as confirmed by FACS analysis (Supplementary Fig. 11A-D).

To further elucidate the impact of Nb457 binding with CD4 on CD4 binding to MHC-II, we aligned the Nb457-CD4 complex with the CD4-MHC-II complex, revealing that Nb457 binding sites are situated on the opposite side of MHC-II binding sites, exerting a negligible effect on MHC-II binding (Supplementary Fig. 10C). These findings are in agreement with our experimental data, which demonstrated that Nb457 binding had no obvious impact on CD4 binding to MHC-II on Daudi cells (Supplementary Fig. 12A-B). Taken together, the binding sites of Nb457 predominantly reside at the junction of D1-D2, leading to conformational changes of D1 that hinder gp120 binding and potentially contribute to its potent neutralization of HIV-1.

Nb457-based trimeric nanobodies exhibited enhanced potency against HIV-1 live virus.

In order to mitigate potential side-effects associated with the Fc fusion tag and to extend the *in vivo* half-life of Nb_{457}, we employed a novel trimeric VHH format for Nb_{457}, termed Nb_{457}-Nb_{HSA}-Nb_{457} (Fig. 5A), following a novel strategy developed in our laboratory[14]. This novel construct strategically targets CD4 protein through Nb457, while simultaneously harnessing the binding capacity of Nb_{HSA} towards both human serum albumin (HSA) and murine serum albumin (MSA) proteins, thus offering the potential for improved *in vivo* stability[14]. As expected, the Nb_{457}-Nb_{HSA}-Nb_{457} construct exhibited impressive binding affinities with both CD4 protein and HSA protein, yielding measured KD values of 4.2 nM and 29.4 nM, respectively (Supplementary Fig. 13A-C).

Remarkably, Nb_{457}-Nb_{HSA}-Nb_{457} demonstrated significantly enhanced neutralization activity against live HIV-1 infection when compared to the Nb_{457}-Fc and Ibalizumab. Notably, Nb_{457}-Nb_{HSA}-Nb_{457} effectively neutralized all five representative strains of tested HIV-1 live virus, including tier 1 and tier 2 variants, with an average IC_{50} value of 94.75 ng/ml (1.18 nM) and an average IC_{90} value of 360.9 ng/ml (4.51 nM) (Fig. 5B-G). In contrast, the Nb_{457}-Fc neutralized the same set of HIV-1 live virus strains with an IC_{50} value of 66.9 ng/ml (0.83 nM) and exhibited IC_{90} values ranging from 61.9 ng/ml to 323 ng/ml (0.77–4.03 nM) only for four out of five strains (Fig. 5B-G). As for Ibalizumab, it effectively neutralized all tested HIV-1 live virus strains with an IC_{50} value of 496.2 ng/ml (3.31 nM) and IC_{90} values ranging from 150.8 ng/ml to 2884 ng/ml (1.01–19.2 nM) only for two out of five strains (Fig. 5B-G). In aggregate, Nb_{457}-Nb_{HSA}-Nb_{457},

Nb_{457}-Fc and Ibalizumab achieved 100%, 80% and 40% inhibition, respectively, against live HIV-1 infection at the 90% inhibition level.

Notably, Ibalizumab exhibited neutralization curves that plateaued below complete inhibition for all five strains of the tested live HIV-1 virus, a trend that aligns with previous reports[21] (Fig. 5B-G). Similarly, the Nb_{457}-Fc construct displayed inhibition curves with maximum percent inhibition (MPI) below 100%, specifically against the live HIV-1_{BAL} and HIV-1_{CH058} strains (Fig. 5B-G). Such strains with MPI values below 100% may harbor the potential to elude the inhibitory effects of Ibalizumab or Nb_{457}-Fc. In striking contrast, Nb_{457}-Nb_{HSA}-Nb_{457} achieved the complete neutralization of all five strains of the tested live HIV-1 virus, as evidenced by an MPI value of 100% (Fig. 5B-G). This finding underscores a significantly diminished likelihood of viral escape when employing Nb457-based trimeric nanobodies. In summary, the unique structural arrangement of Nb_{457}-Nb_{HSA}-Nb_{457} demonstrated unequivocally superior neutralization efficacy across the entire spectrum of tested HIV-1 live virus strains, with an MPI value attaining the optimal threshold of 100%.

Molecular Dynamics simulation revealed structural Basis for complete inhibition of HIV-1_{CH058} by Nb457-based trimeric nanobodies

To elucidate the intriguing phenomenon wherein Nb_{457}-Fc exhibited sub-100% inhibition of live HIV-1_{CH058} infection, akin to Ibalizumab, while Nb_{457}-Nb_{HSA}-Nb_{457} demonstrated complete 100% inhibition against HIV-1_{CH058} infection (Fig. 5C), we established three distinct systems: CD4 and gp120 (derived from the HIV-1_{CH058} sequence) (Supplementary Fig. 14A), CD4, gp120 (HIV-1_{CH058} sequence), and Nb_{457}-Fc (Supplementary Fig. 14B), and CD4, gp120 (HIV-1_{CH058} sequence), and Nb_{457}-Nb_{HSA}-Nb_{457} (Supplementary Fig. 14C). Each of these systems underwent a rigorous 500 ns molecular dynamics (MD) simulation, with the final 400 ns chosen for subsequent analysis. Our primary focus was centered on evaluating the CD4 and gp120 interaction, examining two critical aspects: the count of main-chain hydrogen bonds, pivotal in their binding, and the Root Mean Square Fluctuation (RMSF) values specifically concerning the D1-D2 domain of CD4.

We meticulously scrutinized the temporal dynamics of main-chain hydrogen bonds within these three systems. When the tally of hydrogen bonds reached or surpassed 1, it signified an interaction between CD4 and gp120, prompting us to diligently record the conformations at these junctures. Subsequently, we generated histograms to visually represent this data (Supplementary Fig. 13C). Additionally, we computed the mean number of main-chain hydrogen bonds for each system. The system devoid of nanobodies exhibited a mean value of 0.911, while the systems incorporating Nb_{457}-Fc and Nb_{457}-Nb_{HSA}-Nb_{457} displayed mean values of 0.212 and 0.126, respectively. This observation underscores the role of Nb_{457}-Fc and, particularly, Nb_{457}-Nb_{HSA}-Nb_{457} in diminishing the count of main-chain hydrogen bonds in the CD4 and gp120 interaction, with Nb_{457}-Nb_{HSA}-Nb_{457} exerting a more pronounced effect.

Through cluster analysis, we identified the most probable conformations for each system and pinpointed their main-chain hydrogen bonds. In the absence of antibodies, the system featured two primary main-chain hydrogen bonds, specifically between K46 of CD4 and G330 of gp120, and between L44 of CD4 and D332 of gp120 (Supplementary Fig. 14A). In contrast, systems containing Nb_{457}-Fc displayed a single main-chain hydrogen bond, linking K46 of CD4 with G331 of gp120 (Supplementary Fig. 14B). Similarly, for systems encompassing Nb_{457}-Nb_{HSA}-Nb_{457}, we observed a single main-chain hydrogen bond, precisely between Q33 of CD4 and G415 of gp120 (Supplementary Fig. 14C).

Investigation of the impact of anti-CD4 Nbs on $CD4^+$ T cells

To assess the impact of Nb457 on CD4 binding with MHC II, we initially incubated CD4-rFc protein with Nbs and subsequently evaluated its binding with MHC-II on Daudi cells. The CD4-rFc protein exhibited a dose-dependent binding with Daudi cells, as determined by flow cytometry (Supplementary Fig. 12A). Remarkably, control Nb, Nb_{457}-Fc, Nb_{457}-Nb_{HSA}-Nb_{457}, and Ibalizumab at concentrations ranging from 0.03 to 2 μg/ml revealed no discernible impact on CD4 binding with MHC-II on Daudi cells (Supplementary Fig. 13B), which agreed with the structural analysis (Supplementary Fig. 10C).

To evaluate the effects of Nb457 on T cell proliferation, we incubated PBMCs from healthy donors, with or without PHA stimulation, along with Nb457 and control Nbs for 4 days. Intracellular expression of the cell proliferation marker Ki67 was measured by flow cytometry. Compared to unstimulated conditions, Ki67 expression was significantly increased with PHA stimulation (Supplementary Fig. 15A). Notably, the results demonstrated that treatments with control Nb, Nb_{457}-Fc, Nb_{457}-Nb_{HSA}-Nb_{457}, and Ibalizumab did not show any significant difference in Ki67 expression in $CD4^+$ T cells under both PHA stimulation and unstimulated conditions (Supplementary Fig. 15A). These findings suggest that Nb_{457}-Fc and Nb_{457}-Nb_{HSA}-Nb_{457} do not exhibit any discernible impact on $CD4^+$ T cell proliferation.

As a quantitative measure of T cell activation, we conducted an evaluation of an early activation marker (CD69) and the interleukin (IL)-2 receptor α chain (CD25) on $CD4^+$ T cells (Supplementary Fig. 15B-C). Remarkably, across samples from the same donor and stimulation, we observed highly similar activation profiles for all Nb treatments. The percentage of $CD4^+CD25^+$ cells steadily increased over time under PHA-stimulated condition, with the percentage of positive cells consistently remaining high at all analytic points (Supplementary Fig. 15B-C). Importantly, irrespective of inter-donor variations, treatments with Nb457, Ibalizumab or control Nb did not result in significant differences in the percentage of $CD4^+CD25^+$ or $CD4^+CD69^+$ cells under both conditions of PHA stimulation and unstimulated conditions (Supplementary Fig. 15B-C).

Subsequently, we conducted an analysis of cytokine expression in $CD4^+$ T cells through intracellular cytokine staining. Samples were treated with different antibodies with or without PHA stimulation. Notably, samples treated with control Nb, Nb_{457}-Fc, Nb_{457}-Nb_{HSA}-Nb_{457} and Ibalizumab exhibited remarkably similar percentages of cytokine expression, including IL-2, IFN-γ, and tumor necrosis factor (TNF-α) under either PHA stimulation or unstimulated conditions (Supplementary Fig. 15D-F).

Taken together, our findings demonstrated that exposure to Nb_{457}-Fc or Nb_{457}-Nb_{HSA}-Nb_{457} did not exert any significant impact on MHC-II binding with CD4, proliferation, activation, or cytokine production of $CD4^+$ T cells. These results highlight the safety and potential therapeutic value of Nb_{457}-Fc or Nb_{457}-Nb_{HSA}-Nb_{457}.

Therapeutic efficacy of Nb457 treating HIV-1-infected humanized NDG-HuPBL mice

To assess the *in vivo* efficacy of Nb457 in treating HIV-1 infection, a humanized mouse model (NDG-HuPBL) with HIV-1 infection was established following our established protocols[8] (Fig. 6A). These mice were challenged with 10 pg of P24 HIV-1_{CH058}, originating from a transmitted/founder virus, known to be a tier 2 virus, and exhibiting resistance to most antibody neutralization[22]. Notably, neutralization assays revealed potent inhibition of HIV-1_{CH058} by Nb_{457}-Fc, Nb_{457}-Nb_{HSA}-Nb_{457} and Ibalizumab. However, both Nb_{457}-Fc and Ibalizumab failed to achieve complete neutralization even at the highest doses. In contrast, Nb_{457}-Nb_{HSA}-Nb_{457} demonstrated remarkable efficacy, achieving 100% inhibition at 246.9 ng/ml (Fig. 5C and 5G).

Given that intraperitoneal (*i.p.*) administration of Nb457 resulted in a rapid attainment of peak serum concentration (C_{max}) but with a short half-life, while subcutaneous (s.c.) administration necessitated a longer time to reach Cmax but conferred a longer half-life (Supplementary Fig. 16A-C), we adopted a combination approach for evaluating Nb457 *in vivo*. As such, to evaluate the therapeutic effects, we administered 400 μg/mouse of each antibody via *i.p.* plus *s.c.* routes to HIV-1 infected NDG-HuPBL mice (n = 4) at 1 day, 3 days, 5 days, and 7 days post-infection (Fig. 6A). The viral load in blood was monitored on a weekly basis for four weeks post-infection and revealed a progressive increase in the control group, while the treatment groups displayed significantly lower viral loads compared to the Nb Ctl group. Notably, the Ibalizumab and Nb_{457}-Nb_{HSA}-Nb_{457} groups exhibited substantial reductions in viral loads by 2 to 5 logs at 3 and 4 weeks post-infection (Fig. 6B). To further validate the viral load, we isolated spleenocytes from sacrificed mice and cultured them *ex vivo* for two days, followed by viral RNA quantification in cell supernatants. Viral RNA levels in cell supernatants from Nb457 or Ibalizumab-treated mice were significantly lower compared to the control Nb treatment (Fig. 6C). Notably, 2/4 cell supernatants from the Nb_{457}-Nb_{HSA}-Nb_{457}-treated group exhibited undetectable viral RNA, in agreement with the viral RNA levels in the blood (Fig. 6B-C). Immunofluorescence staining of P24 in the spleen corroborated these findings, showing reduced $P24^+$ positive cells in Nb457-Fc or Ibalizumab-treated groups, and only a scattered and limited presence of $P24^+$ positive cells in mice treated with Nb_{457}-Nb_{HSA}-Nb_{457} (Fig. 6D).

In conclusion, our study demonstrated the robust inhibitory effects of Nb_{457}-Nb_{HSA}-Nb_{457}, along with Nb_{457}-Fc and Ibalizumab, on HIV-1 replication *in vivo*. Notably, Nb_{457}-Nb_{HSA}-Nb_{457} exhibited outstanding efficacy, as evidenced by the VOA assay and immunostaining of the spleen.

Discussion

The development of effective therapies for HIV-1 infection remains a formidable challenge. Ibalizumab, the sole antibody drug with specific binding to CD4, has demonstrated therapeutic efficacy against multidrug-resistant HIV-1 isolates[6,7], highlighting CD4 as a promising target for HIV-1 drug development. However, the limited breadth, potency and MPI less than 100% of Ibalizumab pose challenges for long-term treatment and raise concerns about the potential to the development of antibody resistance. Clearly, more potent and broadly effective antibodies are needed. This can be achieved either by isolating antibodies with exceptional neutralizing activity using new strategies or engineering existing antibodies into bi- or tri-specific combinations. Previously, we reported the development of the bispecific antibody BiIA-SG, which combines two single-chain variable fragment (scFv) binding domains of Ibalizumab and the broadly neutralizing antibody PGT-128, targeting HIV gp120[8,9]. BiIA-SG significantly improved the breadth and potency of Ibalizumab and provided functional cure in humanized mouse and macaque models[8,9], further highlighting the potential of CD4 antibodies in the development of novel HIV-1 therapeutics.

In recent years, nanobodies have emerged as a promising alternative to traditional antibodies for drug development owing to their unique advantages. While several anti-CD4 nanobodies have been developed for tracing CD4 cells *in vivo*[20], their potential as therapeutics for neutralization against HIV-1 infection has yet to be explored. To address this gap, we isolated a panel of anti-CD4 nanobodies from an alpaca immunized with human CD4, and found that Nb457 in particular has significant potential as a therapy for HIV-1 infection. Our extensive neutralization testing, encompassing 93 different HIV-1 isolates, which included 35 isolates assessed at Nanjing University and additional 58 isolates evaluated at Tsinghua University, revealed that Nb457 had both significantly superior neutralizing potencies and a much broader spectrum of activity against HIV-1 than Ibalizumab, which was more potent than those of the broadly neutralizing monoclonal antibodies PG9 and VRC01[7]. Specifically, the IC_{90} of Nb457 was 0.6 μg/ml, with a neutralization of 91.4% of the isolates, indicating that the potency and broad activity of Nb457 is nearly 5 times and 90% higher than Ibalizumab, respectively. Notably, among the reported anti-HIV antibodies with ultrapotent neutralization capacity[23–26], Nb457 stands out with one of the lowest IC_{90} values, underscoring its exceptional potency. Furthermore, its broad-spectrum activity against over 90% of the isolates suggests that HIV-1 is less likely to develop resistance to Nb457. Thus, Nb457, as the first alpaca-derived nanobody binding to CD4, represents an ultra-potent and highly broadly neutralizing nanobody against diverse HIV-1 genotypes.

An intriguing finding was observed when comparing trimeric Nb457 (Nb_{457}-Nb_{HSA}-Nb_{457}) with Ibalizumab and Nb_{457}-Fc. Ibalizumab demonstrated inhibition curves with MPI values consistently below 100% across all five live HIV-1 strains tested, while Nb_{457}-Fc exhibited similar MPI values but only against the HIV-1_{BAL} and HIV-1_{CH058} strains. In stark contrast, our engineered Nb457-based trimeric nanobodies, Nb_{457}-Nb_{HSA}-Nb_{457}, displayed complete neutralization of various HIV-1 live strains, achieving an MPI value of 100%. This exceptional outcome strongly suggests a significantly reduced likelihood of viral

escape when utilizing Nb_{457}-Nb_{HSA}-Nb_{457} nanobody. These findings underscore the potential of trimeric nanobodies as a promising therapeutic agent for HIV-1 treatment. Further studies are warranted to explore the clinical utility of nanobodies and their broader applications in combating HIV-1 infection.

The identification of ultrapotent and broadly neutralizing anti-CD4 nanobodies, exemplified by Nb457, represents a significant breakthrough in the development of novel therapeutics against HIV-1. Structural analysis of Nb457 revealed its binding affinity to the D1D2 domain of CD4, leading to conformational changes that effectively hinder the binding of gp120 to CD4 and, consequently, inhibit HIV-1 entry into host cells. The epitope of Nb457 was found to partially overlap with that of Ibalizumab, albeit situated on the opposite side of MHC-II binding sites, which exerted no adverse effects on MHC-II binding. Importantly, our experimental results demonstrated that exposure to Nb457 did not interfere with MHC-II binding, proliferation, activation, or cytokine production of $CD4^+$ T cells, highlighting the favorable safety profile of Nb457.

In vivo studies conducted in humanized mice have demonstrated the therapeutic efficacy of Nb457 against HIV-1 infection, even when administered subcutaneously. Notably, the application of trimeric nanobodies has shown superior efficacy, further accentuating the potential of these nanobodies as promising therapeutics. Particularly, in the Nb_{457}-Nb_{HSA}-Nb_{457} trimeric nanobodies group, some mice achieved an almost undetectable viral load, as assessed through Q-PCR, VOA, and immunofluorescence staining. These results underscore the efficacy of Nb457 as an effective inhibitor of HIV-1 infection *in vivo*, with Nb_{457}-Nb_{HSA}-Nb_{457} trimeric nanobodies demonstrating significantly enhanced therapeutic efficacy for the treatment of HIV-1 infection *in vivo*. These findings underscore the potential of Nb457 as a promising candidate, offering high efficacy in targeting a diverse range of clinical HIV-1 variants, including drug-resistant strains.

The unique properties of nanobodies, including their small size, high thermal stability, and specificity, make them well-suited for a range of biomedical applications, offering a promising avenue for the development of innovative HIV-1 therapeutics. For instance, CD4 nanobodies hold promise for gene therapy applications, enabling in vivo delivery of the CD4 nanobody gene. Additionally, they may find utility in CD4 CAR-T gene therapy, leveraging their specific targeting capabilities for enhanced therapeutic outcomes. Furthermore, CD4 nanobodies conjugated with drugs could be developed as ADCs, serving as a platform for new drug development based on the properties of Nb457. In addition, the small molecular mass of nanobody makes higher molar production of nanobody per culture unit and the simpler structure allows the production in yeast or bacterial system feasible, which will significantly reduce the cost to the end users, a critical restricting factor for broader application of the antibody-based HIV-1 therapy.

In conclusion, our study represents a significant advancement in the development of ultra-potent anti-CD4 nanobodies as promising therapeutics against HIV-1 infection. The distinct properties exhibited by Nb457, including its non-interference with MHC-II binding and T cell function, alongside its exceptional efficacy against diverse HIV-1 strains, position it as a compelling candidate for further research and therapeutic applications. Importantly, Nb_{457}-Nb_{HSA}-Nb_{457} demonstrated robust protection in some HIV-

infected humanized mice, attaining an MPI of 100%, further underscoring its potential as a highly effective candidate for targeting a wide array of clinical HIV-1 variants, including drug-resistant strains.

Materials and Methods

1. Alpaca Immunization

The Alpaca immunization procedure was conducted with some adjustments based on our previously published method [27]. Briefly, one alpaca received an initial immunization comprising 250 µg of CD4-rFc protein emulsified with 250 µl of Freund's complete adjuvant (Cat#: F5881-10ML, Sigma). Subsequently, three additional boosts were administered at weeks 2, 4, and 6, each consisting of 250 µg of CD4-rFc protein diluted in 250 µl of Freund's incomplete adjuvant (Cat#: F5506-10ML, Sigma). Blood samples were collected for anti-serum characterization with CD4-His one week following both the 3rd and 4th immunizations. Furthermore, 100 ml of blood was collected one week after the 4th immunization for anti-serum characterization and to develop a phage library displaying the VHH antibody.

2. SDS-PAGE and Western blotting:

Recombinant proteins, engineered with either a rabbit Fc (rFc) tag or His-tag at the C-terminus, were transiently expressed in FreeStyleTM 293-F cells (Cat#: R79007, Thermo Scientific) and subsequently purified from the cell culture supernatant. Commercial Protein A Sepharose (Cat#: 20334, Thermo Scientific) or Ni-NTA (Cat#: R901100, Thermo Scientific) columns were employed for purification, depending on the protein variant. Post-purification, proteins or antibodies were resolved using electrophoresis on a 7.5%-12% polyacrylamide gel. Electrophoresis was conducted under reducing and nonreducing conditions to discern the absence and presence of β-mercaptoethanol in the gel-loading buffer, respectively. Protein bands were visualized through either Coomassie blue staining or were transferred onto a PVDF membrane for immunoblotting. After membrane blocking, incubation ensued with the respective antibodies or plasma, either at 4 ^{o}C overnight or at 37 ^{o}C for 60 minutes. Subsequently, a secondary antibody, specifically anti-rabbit IgG or anti-human IgG, conjugated with an IRDye 800CW (Cat#: 926-32232, Rockland), was utilized. Protein bands were imaged and analyzed using the Odyssey Image System (Li-COR).

3. ELISA for characterizing anti-sera and antibody.

Antibody characterization and the determination of anti-sera titers were conducted using a modified ELISA protocol, previously established in our laboratory [28]. High protein-binding ELISA plates (Cat#: 9018, Corning) were coated with protein at a concentration of 0.5 µg/ml, with 100 µl per well, and incubated at either at 4°C overnight or at 37°C for 2 hours. After washing, plates were blocked with 5% non-fat milk in PBS at 37°C for 60 mins. Subsequently, 100 µl serially diluted anti-sera or purified antibody were added and incubated at 37°C for 1.5 hours. Plates were then washed and incubated with either goat anti-human IgG with HRP (1:10000 dilution, Cat#: 109-035-088, Jackson ImmunoResearch) or goat anti-llama IgG (H + L) secondary antibody with HRP (1:10000 dilution, Cat#: NB7242, Novus) at 37°C for 1 hour. After this

incubation, the 3,3',5,5'-Tetramethylbenzidine (TMB, Sigma) substrate was added and allowed to react at 37°C for 10 mins. The reaction was terminated by adding 10 µl of 0.2 M H2SO4. Optical densities were measured at 450 nm using the Infinite 200 instrument (Tecan, Ramsey, MN, USA). Antibody titers were determined as the highest dilution at which the sample generated an optical density readout at least 2.1-fold higher than the control serum sample at the same dilution.

4. Construction of a phage library displaying VHH antibody

A VHH phage library was established with certain modifications made to a previously documented method [29]. In brief, peripheral blood mononuclear cells (PBMCs) were isolated from 100 ml blood obtained from the immunized alpaca, employing a lymphocyte separation solution (GE Ficoll-Paque Plus, Cat#: 17-1140-02). RNA was extracted and reverse transcribed into cDNA, following the TRIzol kit's instructions, utilizing oligo (dT) and random hexamers as primers. Subsequently, the alpaca VHH gene was amplified using specific primer combinations and then cloned into the phV1 phagemid plasmid (Abrev, Ltd., Nanjing, China) for subsequent transformation into TG1 bacteria.

5. Panning VHH phage library

Affinity selection of CD4-binding recombinant phages was performed using an enrichment protocol, with modifications adapted from a previously described method[30]. Specifically, VHH-phagemid-transformed bacteria were rescued using M13KO7 helper phage (Cat#: 18311019, Invitrogen) and then precipitated using PEG/NaCl. The phage VHH antibody library underwent three rounds of enrichment by incubation with 50 µg/ml of CD4-His protein. The enriched phage pool was subsequently eluted, transformed, and monoclonal phages were selected for evaluation via phage ELISA using CD4 as the target protein. For Phage ELISA, 96-well plates (Cat#: 9018, Corning) were coated with 200 ng of CD4-His protein in a coating buffer (pH 9.6) and incubated at 4°C overnight. The plates were then blocked for 1 hour at 37°C with blocking buffer (3% BSA in PBST), followed by incubation with library phages or single clone phages in bacterial supernatants at 4°C for 1.5 hours. After washing, anti-M13 bacteriophage antibody with HRP (1:10000 dilution, Cat#: 11973-MM05T-H, Sino Biological) was added and incubated at 37°C for 1 hour. Subsequently, 3,3',5,5'-Tetramethylbenzidine (TMB, Sigma) substrate was added and allowed to react at 37°C for 10 minutes, with the reaction being quenched by adding 10 µl of 0.2 M H2SO4. Optical densities were measured at 450 nm using the Infinite 200 instrument (Tecan, Ramsey, MN, USA). Clones exhibiting a readout at 450 nm greater than 0.5 were selected for sequencing.

6. Construction and expression of VHH antibody library

The enriched VHH phage library underwent PCR amplification to yield VHH gene fragments, which were subsequently cloned into the prokaryotic expression vector pComb3X. This step resulted in the establishment of a prokaryotic expression VHH antibody library. The library was induced to express VHH antibodies using IPTG, and the bacterial supernatants were assessed using ELISA with CD4 as the target protein. Positive clones were identified by CD4/Blank ratios > 5.0, and the corresponding bacterial clones were sequenced. Among these colonies, a total of 1920 monoclonal colonies were randomly selected.

The bacterial supernatants from these colonies were evaluated for their potential to neutralize HIV infection.

7. VHH-huFc4 (Nb-Fc) or Ibalizumab eukaryotic expression

To enhance the function and stability of VHH antibodies, the Fc4 gene (CH2-CH3) of human monoclonal antibody was fused with VHH gene and cloned into the pVAX1 eukaryotic expression vector. This approach aimed to improve the half-life, Fc-based function, and purification of the VHH antibody. The resultant constructed VHH-huFc-pVAX1 was then transfected into 293F cells to produce VHH-huFc4 (Nb-Fcs) antibody. Following expression, the antibodies were purified using Protein G (Cat#:20399, Thermo Scientific). Meanwhile, Ibalizumab was constructed within the pVAX1 vector, following the published gene sequence, and was likewise expressed in 293F cells as Nb-Fc for further analysis.

8. Expression and purification of trimeric Nb457

To improve the activity of Nb457, we constructed Nb457 with trimeric Nbs configurations (Nb_{457}-Nb_{HSA}-Nb_{457}) wherein $(GGGGS)_3$ linkers were introduced between Nbs in trimeric forms as our previously reported[14]. The specific nanobody targeting Human Serum Albumin (HSA), Nb_{HSA}, was developed through immunization of an alpaca with HSA [14]. To facilitate protein purification, a 6 x His-tag was fused to the C terminus of the Nbs of trimeric configuration. Subsequently, these trimeric Nb457 were cloned into the pcDNA3.4 eukaryotic expression vector (Invitrogen). The vectors containing the engineered trimeric Nbs were then transfected into 293F cells for the production. To isolate and purify the trimeric Nb457 fused with the His-tag, we employed Ni-NTA affinity chromatography (Cat.# R901100, Thermo Fisher Scientific).

9. Affinity determination by Bio-Layer Interferometry (BLI)

The affinity of antibodies was assessed employing a ForteBio OctetRED 96 BLI system (Molecular Devices ForteBio LLC, Fremont, CA), maintaining a shaking rate of 1,000 rpm at 25°C, in accordance with previously established protocols outlined in reference[14]. To quantify the affinity of nanobodies (Nbs) bearing a human Fc tag, Nb-Fcs were immobilized onto anti-human Fc (AHC) biosensors (Cat# 18-5060, Fortebio) within a kinetic buffer (PBS, 0.02% (v/v) Tween-20, pH 7.0) for a duration of 200 seconds. Subsequently, baseline equilibration was carried out for an additional 180 seconds within the same kinetic buffer. The association phase with CD4 was conducted using a three-fold dilution series spanning concentrations from 300 nM to 0.4 nM, followed by a dissociation phase lasting 180 seconds. After each binding cycle, biosensors were regenerated by three brief pulses of 5 seconds each with 100 mM pH 2.7 glycine-HCL buffer. Data analysis encompassed baseline subtraction, and fitting was performed employing a 1:1 binding model in conjunction with the ForteBio data analysis software. To elucidate the kinetic parameters, including the dissociation constant (KD), association rate constant (Ka), and dissociation rate constant (Kd), a global fitting approach was applied to all collected data.

10. HIV-1 neutralization assay

The Global Panel HIV-1 Env clones were acquired from the NIH AIDS Reagent Program (Cat# 12670)[8]. Additionally, a set of 35 Env clones was generated by us or generously provided by our collaborator (H Shang, China Medical University, Shenyang, China)[31]. To assess the efficacy and breadth of various anti-sera or neutralizing nanobodies or antibodies, a luciferase-based assay was performed using a standard inoculum consisting of 200 $TCID_{50}$ of each pseudovirus as previously described[8], in GHOST(3)-X4R5 (Cat# 3942, NIH AIDS Reagent Program). The neutralizing activity of each anti-serum, nanobodies or antibodies was tested in duplicate with a 3-fold serial dilution. The half-maximal inhibitory concentration (IC_{50}), the eightieth percentile inhibitory concentration (IC_{80}) and the ninetieth percentile inhibitory concentration (IC_{90}) of each Nb or antibody were calculated to determine anti-HIV-1 potency. For live HIV-1 neutralization assessments, we conducted the assay using TZM-bl cells (Cat# 8129, NIH AIDS Reagent Program) and a standardized viral inoculum of 200 $TCID_{50}$.

11. In vivo evaluation of Nbs inhibition of HIV infection in NDG-HuPBL mice

HIV-infected immunodeficient NOD.CB17-Prkdcscidll2rgtm1/Bcgen (NDG) mice were established following our previous protocol[27]. In brief, 1.0 x 10^6 to 1.5 x 10^7 human peripheral blood lymphocyte (HuPBL) were injected intraperitoneally into 4-6-week-old of NDG mice (Biocytogen Co., Ltd., China); blood samples from NDG-HuPBL mice collected after two weeks were subjected to flow cytometry to determine the percentage of human $CD45^+$, $CD3^+$, $CD4^+$ and $CD8^+$. NDG-HuPBL Mice with a proportion of human $CD45^+$ cells exceeding 5% were selected for the study. NDG-HuPBL mice were challenged with 10 ng p24 of live of HIV_{CH058}, originating from a transmitted/founder virus (generously provided by the NIH), known to be a tier 2 virus, and exhibiting resistance to most antibody neutralization[22]. The infected NDG-HuPBL mice (n = 8) were treated with 400 µg of nanobodies per mouse via intraperitoneal (*i.p.*) or subcutaneous (*s.c.*) injection at specified time points. Control nanobodies were administered to infected mice following the same time intervals. Sample Collection and Analysis Blood samples were collected at designated time points for various analyses. The concentration of nanobodies in sera was determined using ELISA. Viral load was monitored by quantitative polymerase chain reaction (qPCR). Ultimately, mice were sacrificed for comprehensive detection of infected cells throughout the body.

12. Viral RNA Quantification via Quantitative Reverse Transcription Polymerase Chain Reaction (qRT-PCR)

Viral RNA extraction was accomplished using the QIAamp viral RNA mini kit (Qiagen). The extracted RNA underwent reverse transcription, yielding 20 µl of complementary DNA (cDNA). The reverse transcription process was executed employing the RT-PCR Prime Script Kit (Takara). This resulting cDNA served as the template for subsequent quantitative RT-PCR (qRT-PCR) analysis. For each qRT-PCR reaction, 8 µl of cDNA was combined with TaqMan Universal PCR Master Mix (Life Technologies), a TaqMan probe (5'-FAM – CTCTCT CCTTCT AGCCTC – MGB-3'), and primers that were bespoke to target the P17 gene of HIV-1 (Forward: 5'-TACTGA CGCTCT CGCACC-3'; Reverse: 5'-TCTCGA CGCAGG ACTCG-3'). Amplification was

conducted in triplicate on an Eppendorf Realplex4 Mastercycler (Eppendorf) under the following cycling conditions: an initial cycle at 50°C for 2 minutes, followed by a cycle at 95°C for 10 minutes, and subsequently 40 cycles at 95°C for 15 seconds and 60°C for 1 minute. Viral titer quantification was determined by referencing the samples against a standard curve generated using RNA extracted from a serially diluted reference viral stock. The assay's limit of detection for live HIV-1 was established at 1000 copies per ml, attesting to its sensitivity and precision.

13. Flow cytometry analysis

Blood samples were collected aseptically from the facial veins of mice into Eppendorf tubes containing 50 µl of anti-coagulant (0.5 M EDTA). Subsequently, the samples were centrifuged at 1,150 g for 5 minutes using a microcentrifuge. The resulting plasma was carefully preserved for future analyses, while the cellular pellets were resuspended in 2 ml of 1x RBC lysis buffer (BD Bioscience). Following resuspension, the samples were incubated on ice for 10 minutes to facilitate the removal of red blood cells. Following lysis, the cells underwent a secondary centrifugation step at 1,150 g for 5 minutes at room temperature. The cell pellets were then subjected to immunostaining for a duration of 60 minutes at 4°C using a cocktail comprising 100 µl, which included 2 µl of anti-human CD3-Pacific Blue (Cat# 300442/UCHT1, Biolegend), 2 µl of anti-human CD4-PerCP-Cy5.5 (Cat# 317428/OKT4, Biolegend), 2 µl of anti-human CD8-PE antibodies (Cat# 344706/SK1, Biolegend), and 2 µl of anti-human CD45 PE/Cy7 (Cat# 304016/H130, Biolegend). After staining, the samples were meticulously washed with phosphate-buffered saline (PBS) supplemented with 2% fetal bovine serum (wash buffer). Subsequently, they were centrifuged at 800 g in a microcentrifuge for 5 minutes. The pelleted cells were resuspended in 300 µl of wash buffer and then subjected to analysis. Flow cytometry analysis was performed utilizing a NovoCyte FACS system (Agilent), with data analyzed using FlowJo software version 10.2. Initial gating of samples was carried out based on the expression of human CD45, followed by further analysis of T cell subsets, characterized by the CD3, CD4, and CD8 markers within this gated subset.

14. Immunofluorescence Staining of HIV-Infected Cells in Tissues

Tissues, including the spleen and other tissues, were promptly immersed in 10% neutral buffered formalin for a 24-hour period to ensure optimal fixation. Following fixation, the tissues underwent a transition into 70% ethanol and were subsequently embedded in paraffin. Tissue section with 4 µm in thickness were employed for the Immunofluorescence staining of HIV-p24 using the anti-P24 nanobody fused with rabbit Fc (NbP24-rFc) (Cat# AR0358, Abrev. China), as previously documented[32]. Confocal imaging of these tissue sections was captured using the FV3000 confocal microscope (Olympus), facilitating the acquisition of high-resolution images.

15. Expression and purification of D1-D2 domain of CD4 protein for crystal structural analysis

The recombinant D1-D2 domain of the CD4 protein was expressed using the Bac-to-Bac baculovirus system. The pFastBac1 plasmid, containing the gp67 signal peptide and a C-terminal 6×His tag, was transfected into Sf9 insect cells with Lipofectamine 3000 Reagent (Invitrogen), resulting in the generation of recombinant baculoviruses. Subsequently, these baculoviruses were amplified within Sf9 cells, and after 48 hours post-infection, cell culture supernatants containing the secreted D1-D2 protein were collected. Purification of the D1-D2 protein was conducted through Ni-NTA resin (GE Healthcare) to selectively eliminate nonspecific contaminants. The target protein was eluted using an elution buffer consisting of 20 mM Tris-HCl, 150 mM NaCl, and 300 mM imidazole at pH 7.5. To further improve the purity, a final purification step was conducted using Superdex 200 chromatography (GE Healthcare, USA). The purified proteins were stored in a buffer solution containing 20 mM Tris-HCl and 150 mM NaCl at pH 7.5.

16. Expression and purification of Nb457 for crystal structural analysis

The VHH gene encoding Nb457 was amplified via PCR and subsequently cloned into the pET22b vector using Nco I and Xho I restriction sites. Following cloning, the recombinant plasmids were introduced into Escherichia coli BL21 (DE3) cells. Specifically, the bacterial culture was nurtured in LB medium at 37°C until reaching an optical density at 600 nm (OD_{600}) of 0.6. Protein expression was initiated by the addition of isopropyl-D-1-thiogalactopyranoside (IPTG) to a final concentration of 0.5 mM, and the bacterial culture was incubated at 16°C for 20 hours. The bacterial cells were harvested by centrifugation at 4,500 rpm for 15 minutes and subsequently re-suspended and homogenized in a lysis buffer (20 mM Tris-HCl, 150 mM NaCl, pH 7.5, 10 mM imidazole) utilizing ultrasonication. Following bacterial lysis, the lysate was centrifuged at 18,000 rpm for 30 minutes, and the resulting supernatant was applied to Ni-NTA resin (GE Healthcare, USA) for protein purification. The proteins were eluted with a buffer containing 300 mM imidazole, 20 mM Tris-HCl, and 150 mM NaCl. Further purification was conducted using Superdex 200 chromatography (GE Healthcare, USA) to ensure the highest level of protein purity for subsequent crystal structural analysis.

17. Crystallization, structural determination and data acquisition

The D1D2-Nb457 complexes were generated by mixing the components at a 1:1.5 molar ratio, followed by incubation at 4°C overnight. Crystals of the complexes were grown using the vapor-diffusion sitting-drop method at 16°C, reaching their final size within 3 days in a crystallization solution consisting of 0.1M sodium cacodylate trihydrate at pH 6.8 and 1.4M sodium acetate trihydrate. For data collection, a single crystal was mounted on a nylon loop and flash-cooled with a nitrogen gas stream at 100 K. Diffraction data for D1D2-Nb457 were collected at Shanghai Synchrotron Radiation Facility (SSRF) on BL19U1 using a wavelength of 0.97853 Å. Data processing and scaling were carried out using the HKL3000 package and autoPROC. Molecular replacement (MR) utilized the PHASER program with reference structures (PDB code: 1CDH and 5LHR), and model refinement was performed within the

modified experimental electron density using COOT and PHENIX. Structural figures were created with PyMOL, and epitope and paratope residues, along with their interactions, were identified using PISA at the European Bioinformatics Institute.

18. Assessment of Nb457's Influence on CD4 Binding to Cell Surface MHC-II

The interaction between CD4 protein and MHC-II protein on the surface of Daudi cells was examined following established protocols [33]. CD4 protein fused with rabbit Fc (CD4-rFc) was prepared at varying concentrations (ranging from 0.01 ug/ml to 2.2 ug/ml). Subsequently, 1 x 10^6 Daudi cells were separately incubated with CD4-rFc at 4°C for 30 minutes. Following incubation, cells were subjected to two washes with PBS and subsequently incubated at 4°C for 20 minutes with Alexa Fluor® 488 AffiniPure Goat Anti-Rabbit IgG (H + L) (1:500 dilution) (cat# 128-545-160, Jackson ImmunoResearch). After washes, flow cytometry was utilized for subsequent analysis.

Based on the experimental findings, the linear concentration range for the binding of CD4-rFc to MHC-II on the surface of Daudi cells was determined. CD4-rFc protein, at the concentration established within the linear range, was then incubated with nanobodies or antibodies at 20-fold concentrations at 4°C for 2 hours. Subsequently, 1 x 10^6 Daudi cells were transferred to round-bottomed well plates, centrifuged, washed once with PBS, and then incubated with the mixture of the aforementioned protein and antibodies at 4°C for 30 minutes. After washes, cells were incubated at 4°C for 20 minutes with Alexa Fluor® 488 AffiniPure Goat Anti-Rabbit IgG (H + L) (1:500 dilution) (cat# 128-545-160, Jackson ImmunoResearch). Following washes, flow cytometry was employed for subsequent analysis.

19. Model construction: To facilitate subsequent molecular dynamics simulations, we diligently crafted three pivotal molecular structures: Nb_{457}-Fc, Nb_{457}-Nb_{HSA}-Nb_{457}, and the HIV-1_{CH058} gp120. Our foundational structure for Nb_{457} (PDB ID: 8W90) was previously elucidated in this study, and we complemented this with the acquisition of the Fc structure from the Protein Data Bank (PDB ID: 5dk3). These crucial templates underwent meticulous modeling within the MODELLER framework, employing homology modeling techniques, resulting in the precise construction of the Nb_{457}-Fc structure. Leveraging the conspicuous amino acid sequence homology between Nb_{457} and Nb_{HSA}, we conducted precise homology modeling using SWISS-MODEL [34], culminating in the formation of the Nb_{HSA} structure. Subsequently, we harnessed MODELLER once more, orchestrating the integration of both Nb_{457} and Nb_{HSA} structures, thus achieving the comprehensive Nb_{457}-Nb_{HSA}-Nb_{457} configuration. Significantly, to address the formidable challenge arising from substantial sequence disparities between extant gp120 structures and the unique variant structure of HIV-1_{CH058} gp120, which was evaluated in our live HIV-1 neutralization assay, we harnessed the advanced capabilities of AlphaFold2 [35], a state-of-the-art deep learning methodology, to accurately predict the intricate architecture of our target gp120 derived from HIV-1_{CH058}.

20. Molecular Dynamics Simulations: To gain insight into the mechanisms underlying the actions of Nb_{457}-Fc and Nb_{457}-Nb_{HSA}-Nb_{457}, we established three distinct systems: one devoid of antibodies (comprising only CD4 + gp120), another incorporating Nb_{457}-Fc (denoted as Nb_{457}-Fc + CD4 + gp120), and a third encompassing Nb_{457}-Nb_{HSA}-Nb_{457} (referred to as Nb_{457}-Nb_{HSA}-Nb_{457} + CD4 + gp120). The preparation of these systems was meticulously executed using CHARMM-GUI. Subsequent molecular dynamics (MD) simulations were conducted on each system, employing the GROMACS 2023 package. The force field utilized for all systems was CHARMM36m, accompanied by the TIP3P water model [36]. Neutralization of protein charges was achieved by introducing a 150 mM salt concentration of sodium chloride. The MD simulations were carried out within periodic boundary conditions, employing the NpT ensemble, with temperature maintained at 303 K and pressure set to 1 bar. Prior to the commencement of MD simulations, all systems underwent a 5,000-step energy minimization protocol. Subsequently, MD simulations, with position restraints applied to the protein backbone atoms, were executed for 125 ps, serving as a pre-equilibration step before the 500 ns production MD simulations. To assess the dynamics of the systems, we conducted Root Mean Square Fluctuation (RMSF) analysis, hydrogen bond analysis, and cluster analysis, utilizing built-in programs within GROMACS, namely rmsf, hbond, and cluster.

21. Hydrogen Bond Analysis: To analyze the influence of Nb_{457}-Fc and Nb_{457}-Nb_{HSA}-Nb_{457} on the CD4-gp120 interaction, we conducted an in-depth examination of main-chain hydrogen bonds between CD4 and gp120. Utilizing the hbond analysis module in GROMACS, we generated time-dependent profiles of main-chain hydrogen bond occurrences within each system. Subsequently, employing cluster analysis within GROMACS, we identified the conformation exhibiting the highest frequency as the most probable configuration. The corresponding PDB file for this configuration was then imported into Chimera for comprehensive visualization and further analysis, specifically focusing on the main-chain hydrogen bonds formed [37].

22. PBMC Culture and Stimulation

PBMCs were thawed and treated with Universal Nuclease (Cat# 20156ES25, Yeasen, China) at a final concentration of 12 U/ml for 2 hours at 37°C. Subsequently, cells were gently washed with complete culture medium (RPMI 1640 medium, Life Technologies). The cells were then incubated with nanobodies or antibodies at a concentration of 20 ug/ml at 37°C. The culture medium used was RPMI 1640 supplemented with 10% FBS and 100 U/ml of IL-2, with or without 1×PHA (Cat# 00-4977-93, Ebioscience). All cultures were maintained at 37°C in a 5% CO_2 incubator.

23. Intracellular Cytokine Analysis

Following 40 hours of culture, 5 μg/ml Brefeldin A (Cat# 2031560, BioGems) was added into the treated PBMC. After an additional 8 hours, cells were harvested, and cytokine levels were assessed. Extracellularly, cells were stained with fluorescently labeled antibodies, including anti-CD3 Pacific Blue (UCHT1, Biolegend), anti-CD4 PE-Cy7 (OKT4, Biolegend), anti-CD8 PE (SK1, Biolegend), and Fixable Viability dye (Cat# 65-0866-14, Ebioscience). Incubation was conducted for 20 minutes at 4°C. Subsequently, cells were washed, fixed, and permeabilized using BD Cytofix/Cytoperm solution (Cat#

554714, BD Biosciences) following the manufacturer's instructions. Intracellular staining was performed for anti-TNFα BV786 (Mab11, Biolegend), anti-IL-2 APC (MQ1-17H12, BD), and anti-IFN-γ FITC (4S.B7, BD). Following washes, samples were analyzed by flow cytometry.

24. Cell Proliferation and Activation Assessment

After three days of culture, cells were harvested, and extracellular staining was performed using anti-CD4 PE-Cy7 (OKT4, Biolegend), anti-CD8 PE (SK1, Biolegend), and Fixable Viability dye (Cat# 65-0866-14, Ebioscience). Incubation was carried out for 20 minutes at 4°C. Following washes, cells were fixed with BD permeabilization buffer and subjected to intracellular staining using anti-Ki67 Pacific blue (RUO, Biolegend) for 30 minutes at 4°C. After washes, samples were analyzed using flow cytometry.

25. Pharmacokinetics (PK) of Nb457 and Ibalizumab in vivo

Purified Nb457 nanobodies were administered to NDG-HuPBL (Biocytogen Co., Ltd., China) via intraperitoneal (*i.p.*) or subcutaneous (*s.c.*) injection with 400 μg per mouse (average 20 mg/kg). The quantification of Nb457 or control antibodies levels in serum was accomplished by ELISA. To determine the half-life (T1/2) of Nb457 and Ibalizumab, we applied the equation $T1/2 = \ln(2)/k$, where 'k' represents the rate constant, reciprocally expressed in units corresponding to the x-axis time, derived from a one-phase decay equation using GraphPad software.

26. Statistical analysis

Graphs were generated using GraphPad Prism 5.01 software (GraphPad) or OriginPro 8.5 software (OriginLab). One-way or two-way ANOVA was performed for group comparisons. $P < 0.05$ was considered as statistically significant with mean ± SEM or mean ± SD or median + range.

27. Study approval

The experimental procedures conducted within this research were rigorously approved by the Center for Public Health Research, Medical School, Nanjing University. All protocols pertaining to animals infected with HIV were executed within Biosafety Level 3 animal facilities, meticulously aligning with the recommendations for the ethical care and utilization of animals as specified by the Institutional Review Board of Wuhan Institute of Virology, Chinese Academy of Sciences. All authors declare their adherence to the publishing ethics in the conduct and dissemination of this study.

Declarations

Authors' contributions

XW and LZ conducted most experiments, analyzed the data and wrote the draft manuscript. XW, SY and YW conducted the structural analysis. RW and LZ provided technical assistance and conducted the experiments related with pseudovirus neutralization. FN, MY, PY, ML, YL, QH, YL evaluate the efficacy of

Nbs against live HIV-1 virus *in vitro* or *in vivo*. MA, BZ and PZ conducted the molecular dynamics simulation analysis. XW, LZ, CC, LS, SG, JH, DZ, YL HW, provided technical assistance and did most experiments. XW and ZW designed the study, monitored and financially supported the study and revised the manuscript. All authors critically reviewed the draft manuscript and approved the final version.

Acknowledgments: This work was supported by the National Science Foundation of China (NSFC) (No.32370988, 31970149 and U22A20335), the Major Research and Development Project (2018ZX10301406), and Research Foundation of JiangSu Commission Health project (Grant# ZDA2020014).

References

1. Van de Perre, P. *et al.* Eliminating postnatal HIV transmission in high incidence areas: need for complementary biomedical interventions. *Lancet* **397**, 1316-1324, doi:10.1016/S0140-6736(21)00570-5 (2021).
2. Gupta-Wright, A. *et al.* Virological failure, HIV-1 drug resistance, and early mortality in adults admitted to hospital in Malawi: an observational cohort study. *Lancet HIV* **7**, e620-e628, doi:10.1016/S2352-3018(20)30172-7 (2020).
3. Gupta, R. K. *et al.* HIV-1 drug resistance before initiation or re-initiation of first-line antiretroviral therapy in low-income and middle-income countries: a systematic review and meta-regression analysis. *Lancet Infect Dis* **18**, 346-355, doi:10.1016/S1473-3099(17)30702-8 (2018).
4. Haynes, B. F., Burton, D. R. & Mascola, J. R. Multiple roles for HIV broadly neutralizing antibodies. *Sci Transl Med* **11**, doi:10.1126/scitranslmed.aaz2686 (2019).
5. Caskey, M., Klein, F. & Nussenzweig, M. C. Broadly neutralizing anti-HIV-1 monoclonal antibodies in the clinic. *Nat Med* **25**, 547-553, doi:10.1038/s41591-019-0412-8 (2019).
6. Emu, B. *et al.* Phase 3 Study of Ibalizumab for Multidrug-Resistant HIV-1. *N. Engl. J. Med.* **379**, 645-654, doi:10.1056/NEJMoa1711460 (2018).
7. Blair, H. A. Ibalizumab: A Review in Multidrug-Resistant HIV-1 Infection. *Drugs* **80**, 189-196, doi:10.1007/s40265-020-01258-3 (2020).
8. Wu, X. *et al.* Tandem bispecific neutralizing antibody eliminates HIV-1 infection in humanized mice. *J Clin Invest* **128**, 2239-2251, doi:10.1172/JCI96764 (2018).
9. Niu, M. *et al.* Tandem bispecific antibody prevents pathogenic SHIVSF162P3CN infection and disease progression. *Cell Reports* **36**, doi:10.1016/j.celrep.2021.109611 (2021).
10. Harmsen, M. M. & De Haard, H. J. Properties, production, and applications of camelid single-domain antibody fragments. *Applied microbiology and biotechnology* **77**, 13-22, doi:10.1007/s00253-007-1142-2 (2007).
11. Hamerscasterman, C. *et al.* Naturally-Occurring Antibodies Devoid of Light-Chains. *Nature* **363**, 446-448, doi:DOI 10.1038/363446a0 (1993).

12. Jovcevska, I. & Muyldermans, S. The Therapeutic Potential of Nanobodies. *Biodrugs* **34**, 11-26, doi:10.1007/s40259-019-00392-z (2020).
13. Muyldermans, S. in *Annual Review of Animal Biosciences, Vol 9, 2021* Vol. 9 *Annual Review of Animal Biosciences* (eds H. A. Lewin & R. M. Roberts) 401-421 (2021).
14. Wu, X. *et al.* A potent bispecific nanobody protects hACE2 mice against SARS-CoV-2 infection via intranasal administration. *Cell reports*, 109869-109869, doi:10.1016/j.celrep.2021.109869 (2021).
15. Wu, X. *et al.* Short-Term Instantaneous Prophylaxis and Efficient Treatment Against SARS-CoV-2 in hACE2 Mice Conferred by an Intranasal Nanobody (Nb22). *Frontiers in immunology* **13**, 865401, doi:10.3389/fimmu.2022.865401 (2022).
16. Koenig, P. A. *et al.* Structure-guided multivalent nanobodies block SARS-CoV-2 infection and suppress mutational escape. *Science* **371**, 691-+, doi:ARTN eabe6230 /science.abe6230 (2021).
17. Chen, F. F., Liu, Z. H. & Jiang, F. Prospects of Neutralizing Nanobodies Against SARS-CoV-2. *Frontiers in immunology* **12**, doi:ARTN 690742 /fimmu.2021.690742 (2021).
18. Scully, M. *et al.* Caplacizumab Treatment for Acquired Thrombotic Thrombocytopenic Purpura. *N. Engl. J. Med.* **380**, 335-346, doi:10.1056/NEJMoa1806311 (2019).
19. Zheng, F. *et al.* Applications of nanobodies in brain diseases. *Frontiers in immunology* **13**, 978513, doi:10.3389/fimmu.2022.978513 (2022).
20. Traenkle, B. *et al.* Single-Domain Antibodies for Targeting, Detection, and In Vivo Imaging of Human CD4(+) Cells. *Frontiers in immunology* **12**, doi:10.3389/fimmu.2021.799910 (2021).
21. Freeman, M. M. *et al.* Crystal structure of HIV-1 primary receptor CD4 in complex with a potent antiviral antibody. *Structure* **18**, 1632-1641, doi:10.1016/j.str.2010.09.017 (2010).
22. Lucas, J. *et al.* Identification of early-induced broadly neutralizing activities against transmitted founder HIV strains. *Aids* **37**, 43-49, doi:10.1097/QAD.0000000000003371 (2023).
23. Huang, Y. X. *et al.* Engineered Bispecific Antibodies with Exquisite HIV-1-Neutralizing Activity. *Cell* **165**, 1621-1631, doi:10.1016/j.cell.2016.05.024 (2016).
24. Pace, C. S. *et al.* Bispecific antibodies directed to CD4 domain 2 and HIV envelope exhibit exceptional breadth and picomolar potency against HIV-1. *P Natl Acad Sci USA* **110**, 13540-13545 (2013).
25. Walsh, S. R. & Seaman, M. S. Broadly Neutralizing Antibodies for HIV-1 Prevention. *Frontiers in immunology* **12**, doi:ARTN 712122 /fimmu.2021.712122 (2021).
26. Kwong, P. D., Mascola, J. R. & Nabel, G. J. Broadly neutralizing antibodies and the search for an HIV-1 vaccine: the end of the beginning. *Nature Reviews Immunology* **13**, 693-701, doi:10.1038/nri3516 (2013).
27. Wu, X. *et al.* A single-domain antibody inhibits SFTSV and mitigates virus-induced pathogenesis in vivo. *JCI insight* **5**, doi:10.1172/jci.insight.136855 (2020).
28. Wu, X. *et al.* Induction of neutralizing antibodies by human papillomavirus vaccine generated in mammalian cells. *Antibody Therapeutics*, doi:10.1093/abt/tbz004 (2019).

29. Baral, T. N., MacKenzie, R. & Arbabi Ghahroudi, M. Single-domain antibodies and their utility. *Current protocols in immunology / edited by John E. Coligan ... [et al.]* **103**, Unit 2 17, doi:10.1002/0471142735.im0217s103 (2013).
30. Jahnichen, S. *et al.* CXCR4 nanobodies (VHH-based single variable domains) potently inhibit chemotaxis and HIV-1 replication and mobilize stem cells. *Proc Natl Acad Sci U S A* **107**, 20565-20570, doi:10.1073/pnas.1012865107 (2010).
31. Shang, H. *et al.* Genetic and Neutralization Sensitivity of Diverse HIV-1 env Clones from Chronically Infected Patients in China. *Journal of Biological Chemistry* **286**, 14531-14541, doi:10.1074/jbc.M111.224527 (2011).
32. Wu, X. *et al.* Brain Invasion by CD4(+) T Cells Infected with a Transmitted/Founder HIV-1BJZS7 During Acute Stage in Humanized Mice. *Journal of neuroimmune pharmacology : the official journal of the Society on NeuroImmune Pharmacology* **11**, 572-583, doi:10.1007/s11481-016-9654-0 (2016).
33. Doyle, C. & Strominger, J. L. Interaction between CD4 and class II MHC molecules mediates cell adhesion. *Nature* **330**, 256-259, doi:10.1038/330256a0 (1987).
34. Waterhouse, A. *et al.* SWISS-MODEL: homology modelling of protein structures and complexes. *Nucleic Acids Research* **46**, W296-W303, doi:10.1093/nar/gky427 (2018).
35. Jumper, J. *et al.* Highly accurate protein structure prediction with AlphaFold. *Nature* **596**, 583-+, doi:10.1038/s41586-021-03819-2 (2021).
36. Huang, J. *et al.* CHARMM36m: an improved force field for folded and intrinsically disordered proteins. *Nature methods* **14**, 71-73, doi:10.1038/Nmeth.4067 (2017).
37. Sanner, M. F., Olson, A. J. & Spehner, J. C. Reduced surface: An efficient way to compute molecular surfaces. *Biopolymers* **38**, 305-320, doi:Doi 10.1002/(Sici)1097-0282(199603)38:3<305::Aid-Bip4>3.3.Co;2-8 (1996).

Figures

Fig. 1

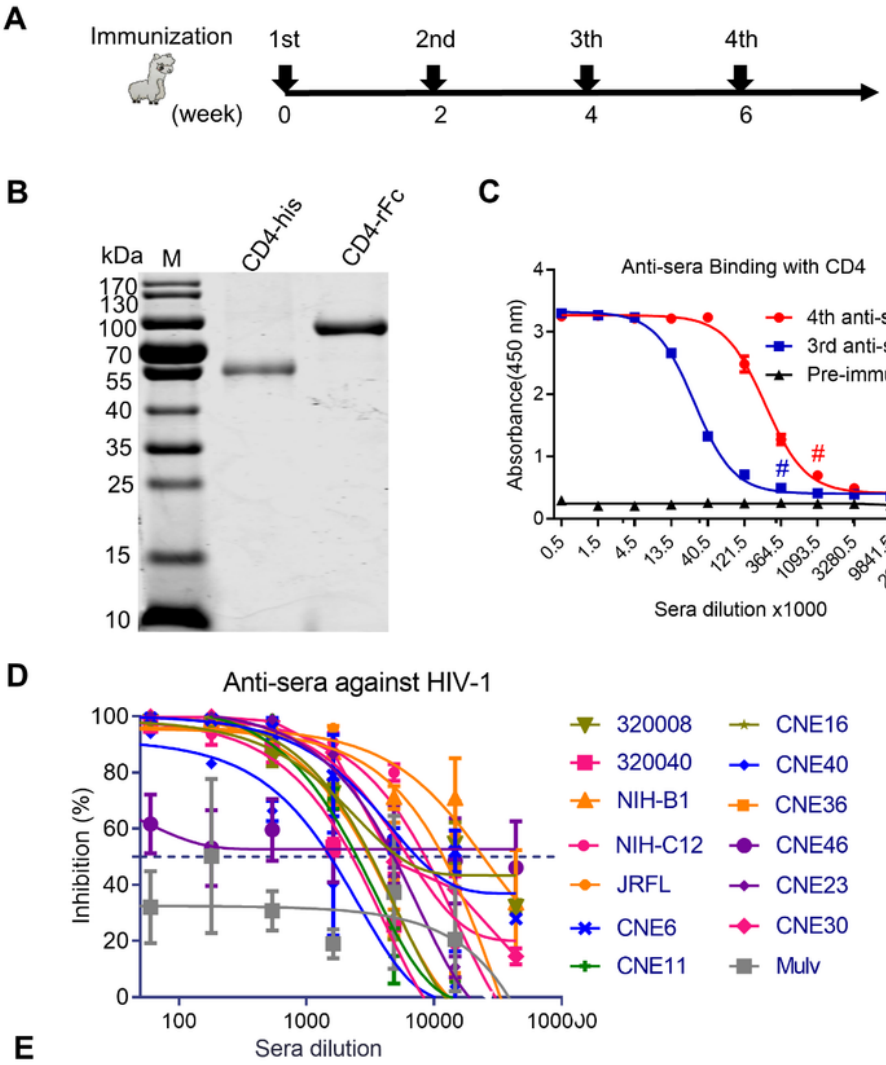

E

Virus	Subtype	Infection stage	R5 or X4	Risk factor	ID_{50}(dilution ratio)		ID_{90}(dilution ratio)	
					Anti-sera	NC	Anti-sera	NC
320008	01AE	Acute T/F	R5	MSM	18524	<20	350	<20
320040	01AE	Acute T/F	R5	MSM	1861	<20	457	<20
NIH-B1	B	Acute T/F	R5	IDU	27026	<20	1189	<20
NIH-C12	B	chronic	R5	?	8347	<20	1764	<20
JRFL	B	chronic	R5	MSM	16421	<20	1828	<20
CNE6	B'	chronic	R5	IDU	15995	<20	779	<20
CNE11	B'	Chronic	R5	Blood	2436	<20	771	<20
CNE16	B'C	chronic	R5	IDU	2963	<20	776	<20
CNE40	07BC	chronic	R5	IDU	1078	<20	90	<20
CNE36	08BC	chronic	R5	IDU	2737	<20	753	<20
CNE46	08BC	chronic	R5	IDU	13037	<20	<20	<20
CNE23	C	chronic	R5	IDU	4102	<20	1187	<20
CNE30	C	chronic	R5	IDU	4623	<20	1235	<20
Mulv	No HIV				<20	<20	<20	<20

Figure 1

Characterization of CD4-induced anti-sera in an alpaca.

(**A**) Experimental schedule of immunization. (**B**) Detection of CD4 protein with His tag (CD4-His) or rabbit Fc tag (CD4-rFc) by SDS-PAGE. (**C**) Evaluation of anti-sera titer after the 3rd and 4th immunization in an alpaca receiving CD4-rFc protein. The y-axis represents the absorbance at 450 nm, and the x-axis shows

the anti-sera dilution fold. Anti-sera binding with CD4-His are labeled on the graph. The terms "3rd anti-sera" and "4th anti-sera" refer to the anti-sera collected one week after the 3rd and 4th immunizations, respectively. (**D**) Neutralizing curve of the 4th anti-sera against the panel of 13 HIV-1 pseudoviruses of various subtypes. Mulv served as the control virus. (**E**) Summary of 50% inhibitory dilution (ID_{50}) and 90% inhibitory dilution (ID_{90}) values, along with the information of pseudoviruses tested in the neutralization assay presented in panel D.

Fig. 2

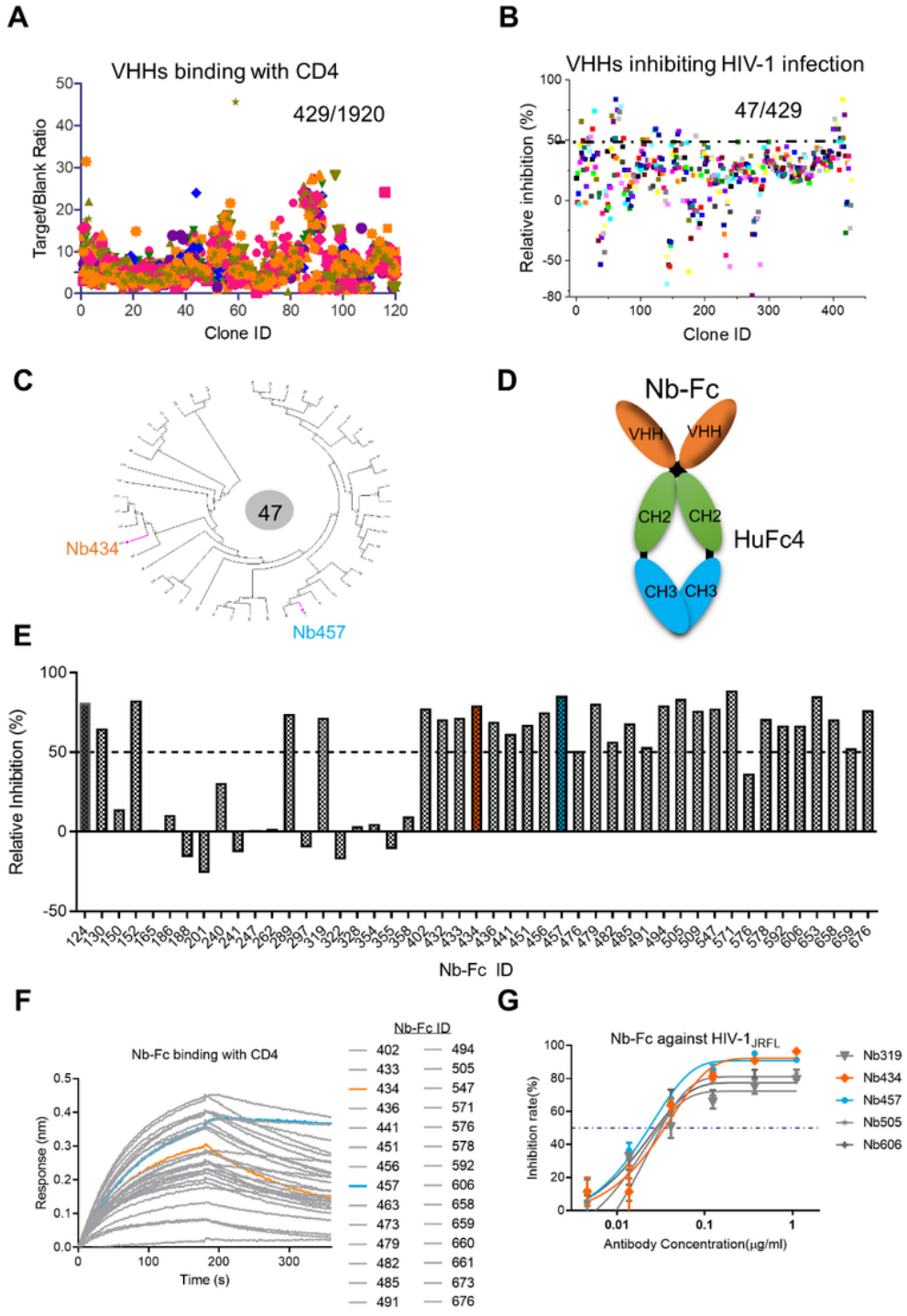

Figure 2

Isolation and characterization of anti-CD4 Nbs. (**A**) Summary of bacterial supernatant binding with CD4 protein tested by phage ELISA. The y-axis represents the ratio of the CD4 binding readout to the blank binding readout. Each dot corresponds to the bacterial supernatant from a single clone among the 1920 clones tested. (**B**) Positive binding VHHs inhibiting HIV-1 infection. Each dot represents one VHH clone supernatant. The dashed line indicates 50% relative inhibition. (**C**) Phylogenetic analysis of the 47 VHHs using the Neighbor-Joining method. The tree is drawn to scale, and branch lengths correspond to the evolutionary distances measured in amino acid substitutions per site. Evolutionary analyses were conducted using the Poisson correction method, with gaps and missing data excluded. MEGA6 software was utilized for the analyses. (**D**) Schematic diagram illustrating the structures of Nb-Fc (nanobody fused with the Fc region), where the VHH is linked to the human Fc4 region (CH2–3). (**E**) Graph depicting the relative inhibition of cell supernatant from 47 various Nb-Fcs tested for neutralization against pseudovirus HIV-$1_{JR\text{-}FL}$ infection. The dashed line represents 50% inhibition. (**F**) Binding curves of 28 Nbs exhibiting interactions with the CD4 protein, as identified by BLI (Biolayer Interferometry), among the 47 various Nbs. (**G**) Neutralizing curve of the five selected Nbs against reference pseudoviruses of HIV-$1_{JR\text{-}FL}$.

Fig. 3

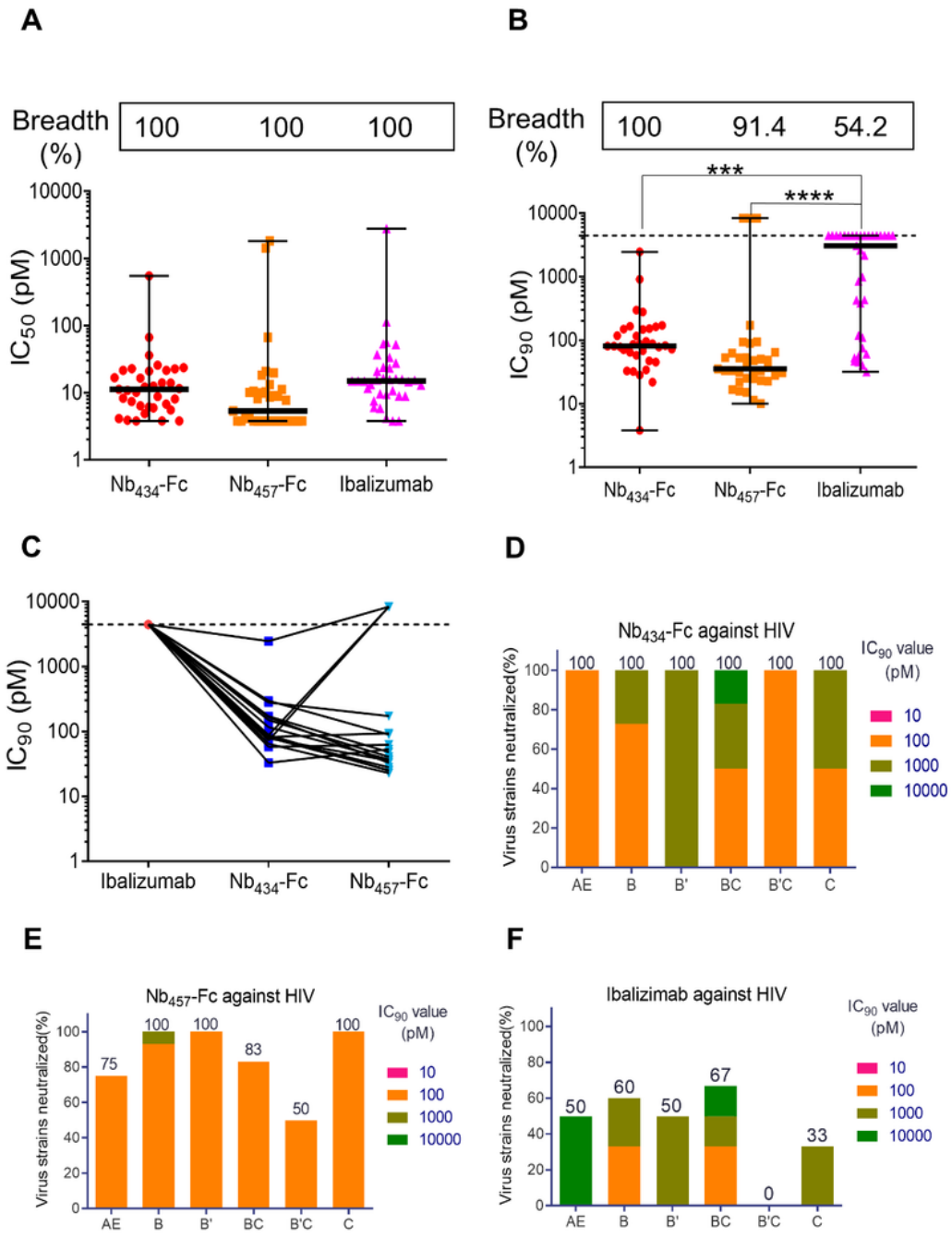

Figure 3

Neutralizing HIV-1 pseudoviruses infection by Nbs. (**A-B**) Graphs depicting the breadth and IC_{50} (A) and IC_{90} (B) values of Nb_{434}-Fc and Nb_{457}-Fc compared with the broadly neutralizing antibody (bnAb) Ibalizumab with the format of whole IgG against the panel of 35 pseudoviruses of various subtypes. Equimolar concentration (pM) was used for comparison, considering the differing molecular weights of Ibalizumab and Nbs. Error bars indicate the mean with 95% confidence interval (CI). One-way ANOVA with

Bonferroni's multiple comparison was used for statistical analysis. ***P < 0.001; ****P < 0.0001. (**C**) Graph illustrating the IC_{90} values of Ibalizumab compared with Nb_{434}-Fc and Nb_{457}-Fc against Ibalizumab-resistant viruses. The analysis is based on the results from panel B. (**D-F**) Graphs showing the IC_{90} values of Nb434 (**D**), Nb457 (**E**), and Ibalizumab (**F**) in neutralizing various subtypes of HIV-1 pseudoviruses infection, as determined by the neutralization results from panel B. The neutralization percentage is indicated in the figure.

Fig. 4

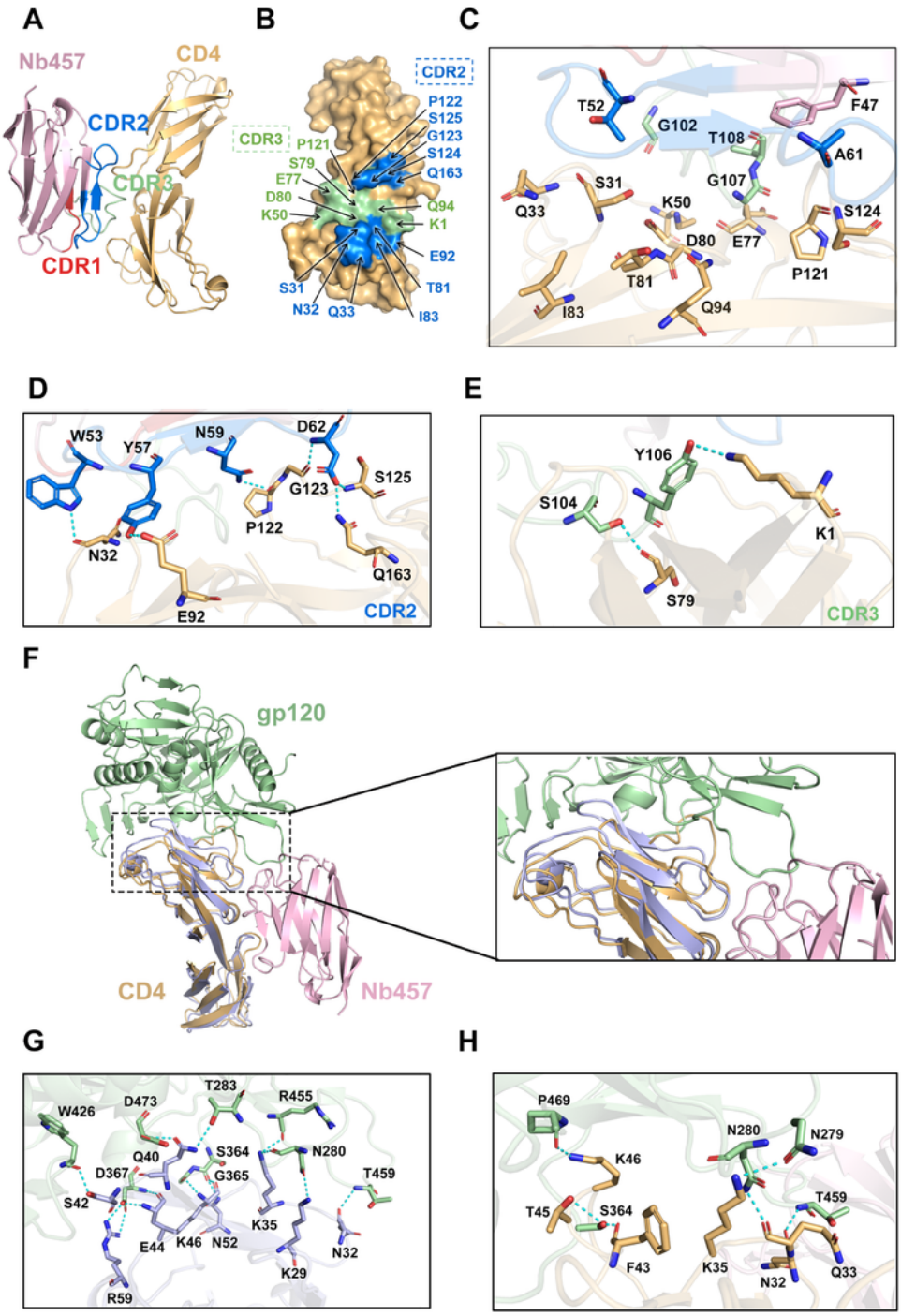

Figure 4

Structural characterization of the Nb457 and CD4 complex. (**A**) Overall configuration of the intricate assembly formed by Nb457 and the D1-D2 domains of CD4. Complementarity Determining Regions (CDRs) of Nb457 are color-coded: CDR1 (red), CDR2 (blue), CDR3 (green), while the D1-D2 domains of CD4 are depicted in orange, utilizing a schematic cartoon representation. (**B**) The epitope of Nb457 shown in surface representation of D1-D2 domains. The regions interacted by CDR2 and CDR3 are colored blue and green, respectively. The key residues were labeled. (**C**) Hydrophobic network between Nb457 and the D1-D2 domains of CD4, elucidated through a representation of amino acid residues in stick conformation. (**D, E**) Elucidation of the interface involving Nb437 and the D1-D2 domains of CD4. CDR regions are differentially color-highlighted in red, blue, and green. Noteworthy interactions within CDR2 (**D**) and CDR3 (**E**) are accentuated, with hydrogen bonding interactions depicted as cyan dashed lines. (**F**) Comparative overlay of the CD4-gp120 (light blue and green) complex and the CD4-Nb457 (orange and pink) complex. Discernible conformational variations in CD4 upon association with Nb457 are juxtaposed against the CD4 arrangement within the gp120-CD4 interface. The inset rectangle magnifies the altered interaction interface. (**G**) Hydrogen bonding schematic at the gp120-CD4 interface, involving a total of 14 hydrogen bonding interactions. (**H**) Elicitation of substantial global structural modifications at the CD4-gp120 junction subsequent to the binding event of Nb457 to CD4. This leads to a discernable reduction in hydrogen bonding interactions from 14 to 6.

Fig. 5

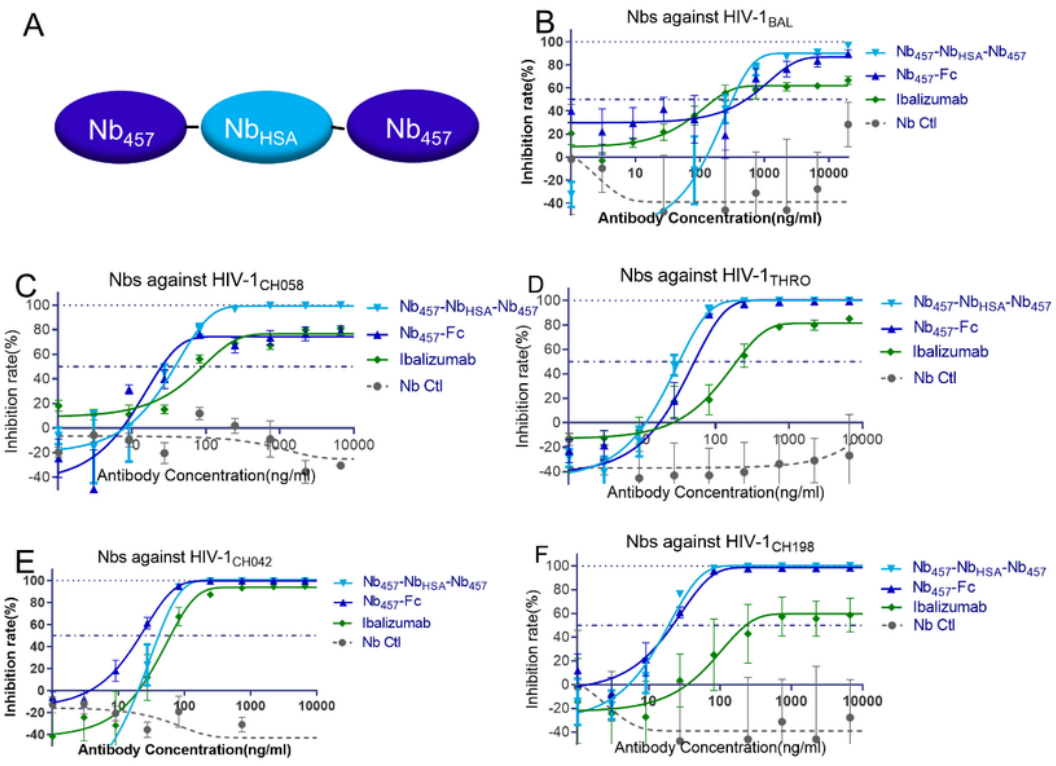

G

Clone ID	ID	Subtype	Tier	ng/ml	Nb_{457}-Nb_{HSA}-Nb_{457}	Nb_{457}-Fc	Ibalizumab	Nb Ctl
BAL	BAL	B	1b	IC_{50}	358.5	179.8	673	>20000
				IC_{80}	696.9	17578	>20000	>20000
				IC_{90}	1028	>20000	>20000	>20000
				IC_{100}	20000	>20000	>20000	>20000
B3	CH058.c /2960	B	2	IC_{50}	34.13	68.82	144.9	>20000
				IC_{80}	62.39	391.9	2573	>20000
				IC_{90}	88.86	1084	>20000	>20000
				IC_{100}	740.74	>20000	>20000	>20000
B7	THRO.c/ 2626	B	2	IC_{50}	27.67	43.96	266	>20000
				IC_{80}	32.16	64.3	1197	>20000
				IC_{90}	34.17	80.31	2884	>20000
				IC_{100}	246.91	740.74	>20000	
C42	CH042.c	C	2	IC_{50}	33.95	21.35	64.03	>20000
				IC_{80}	43.38	41.79	109.9	>20000
				IC_{90}	43.72	61.91	150.8	>20000
				IC_{100}	246.91	246.91	>20000	>20000
C198	CH198.c	C	2	IC_{50}	19.51	20.68	1333	>20000
				IC_{80}	29.14	42.91	>20000	>20000
				IC_{90}	36.84	65.78	>20000	>20000
				IC_{100}	246.91	246.91	>20000	>20000

Figure 5

Neutralizing efficacy of Nb457 against live HIV-1 virus infection. (**A**) Illustration of the schematic structure of Nb_{457}-Nb_{HSA}-Nb_{457}, wherein the trimeric Nbs are interconnected by (G4S)3 linker. (**B-F**) Assessment of the neutralizing effects of Nb457 and Ibalizumab against five distinct live HIV-1 strains: HIV-1_{BAL} (subtype B) (**B**), HIV-1_{CH058} (subtype B) (**C**), HIV-1_{THRO} (subtype B) (**D**), HIV-1_{CH042} (subtype C) (**E**), and HIV-1_{CH198} (subtype C) (**F**). The negative control nanobody, Nb Ctl, was employed. Duplicate data points are

presented as the mean ± standard deviation (SD). Each experiment was independently replicated twice. (**G**) Compilation of IC_{50}, IC_{80}, IC_{90} and IC_{100} values alongside the corresponding data from the neutralization assay performed on live HIV-1 viruses, as detailed in panels B-F.

Fig. 6

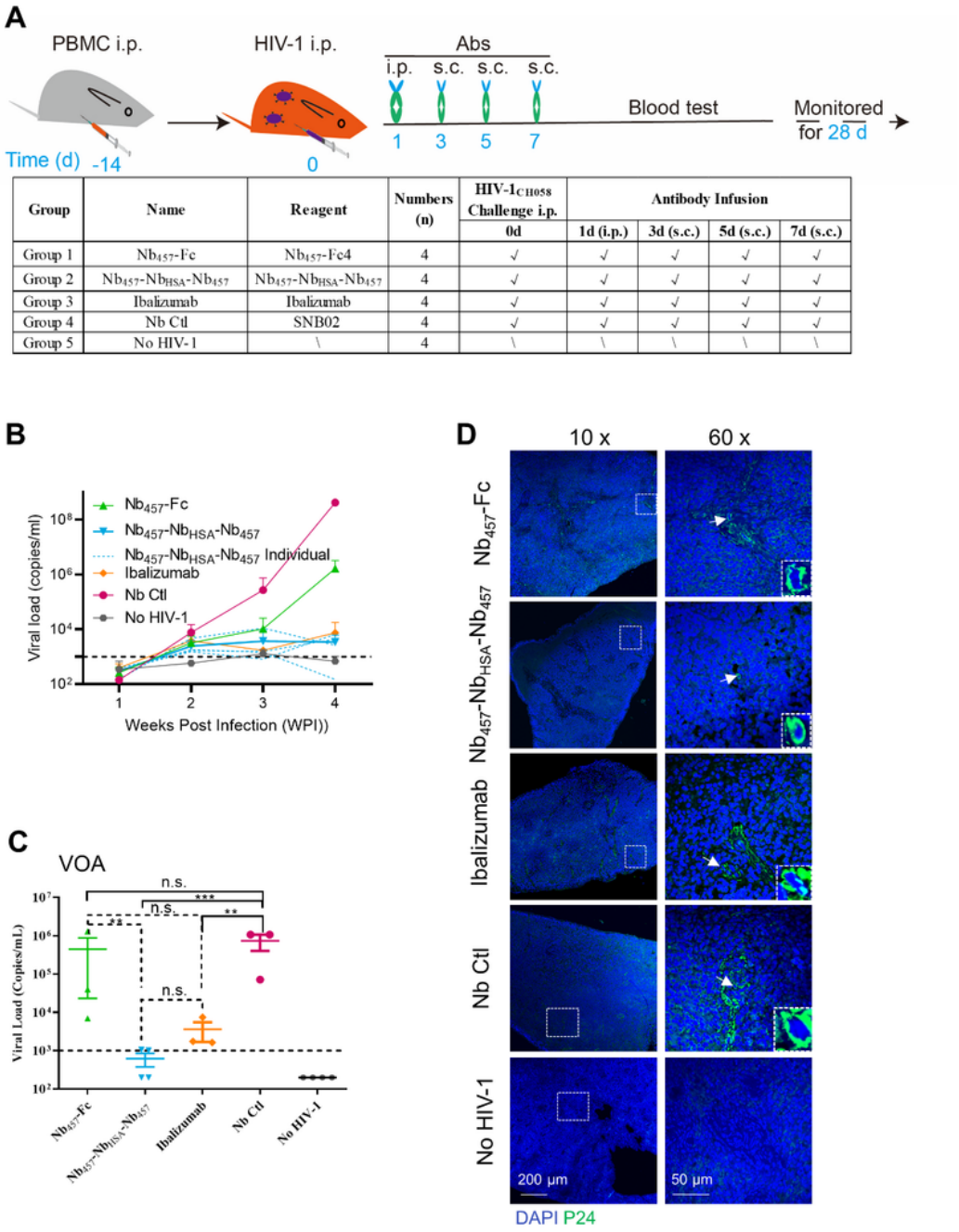

Group	Name	Reagent	Numbers (n)	HIV-1_{CH058} Challenge i.p.	Antibody Infusion			
				0d	1d (i.p.)	3d (s.c.)	5d (s.c.)	7d (s.c.)
Group 1	Nb_{457}-Fc	Nb_{457}-Fc4	4	√	√	√	√	√
Group 2	Nb_{457}-Nb_{HSA}-Nb_{457}	Nb_{457}-Nb_{HSA}-Nb_{457}	4	√	√	√	√	√
Group 3	Ibalizumab	Ibalizumab	4	√	√	√	√	√
Group 4	Nb Ctl	SNB02	4	√	√	√	√	√
Group 5	No HIV-1	\	4	\	\	\	\	\

Figure 6

Therapeutic efficacy of Nb457s in HIV-1-Infected NDG-HuPBL mice.

(**A**) Experimental timeline outlining the immunotherapeutic intervention using Nb457 and Ibalizumab in HIV-1_{CH058}–challenged humanized mice. Intraperitoneal (i.p.) injections were administered at 1 day post-infection (dpi), followed by subcutaneous (s.c.) administrations at 3 dpi, 5 dpi, and 7 dpi after HIV-1 CH058 challenge. Each treatment group received four administrations, including Nb_{457}-Fc, Nb_{457}-Nb_{HSA}-Nb_{457}, Ibalizumab, and a negative control Nb (Nb Ctl, SNB02, one of our published nanobodies specific for envelope protein of SFTSV). The dosage of Nbs or antibodies was 400 μg (~20 mg/kg). The initial HIV-1 inoculum was 10 ng P24. Mice were monitored for four weeks post HIV-1 challenge. A summary of the treatment groups (n = 4 mice) with distinct interventions is presented in the lower table. (**B**) Quantification of plasma viral loads in five groups of NDG-HuPBL mice, color-coded and labeled as in the table in (A), assessed through qRT-PCR. Each line represents data from an individual mouse. (**C**) Viral outgrowth assay (VOA) results of splenocytes from the aforementioned HIV-1-infected NDG-HuPBL mice, indicating viral load in copies per milliliter culture supernatant. (**D**) Immunofluorescence staining of spleen sections using antibodies specific to HIV-1 nucleocapsid protein (P24) in green, and DAPI (4',6-diamidino-2-phenylindole) for nuclei in blue. The green fluorescence intensity was quantitatively analyzed as an indicator of viral infection using ImageJ software. Representative spleen sections were visualized under x10 or x60 objective, with indicated scale bars (200 μm or 50μm), respectively. Data are presented as mean ± standard error of the mean (SEM). Mann-Whitney test was applied to compare the treatment group with the Nb control group. Significance levels: ns, not significant; *$p < 0.05$, **$p < 0.01$, ***$p < 0.001$. Data for (B) and (C) are depicted as mean ± SEM. Experiments in (B) and (C) were replicated twice.

Supplementary Files

This is a list of supplementary files associated with this preprint. Click to download.

- 03CD4NbSupplementalmaterialsandmethods20231008final.docx
- GraphicalAbstract.png